CZECH TECHNICAL UNIVERSITY IN PRAGUE

Faculty of Nuclear Sciences
and Physical Engineering

Department of Dosimetry and Application of Ionising Radiation

MASTER'S THESIS

Parameters affecting radiation-induced plasmid DNA damage

Author: Bc. Zuzana Jamborová
Advisor: Ing. Kateřina Pachnerová Brabcová, Ph.D.
Academic year: 2019/2020

ČESKÉ VYSOKÉ UČENÍ TECHNICKÉ V PRAZE
FAKULTA JADERNÁ A FYZIKÁLNĚ INŽENÝRSKÁ
PRAHA 1 - STARÉ MĚSTO, BŘEHOVÁ 7 - PSČ 115 19

Katedra: KDAIZ *Akademický rok:* 2018/2019

ZADÁNÍ DIPLOMOVÉ PRÁCE

Student:	Bc. Zuzana Jamborová
Studijní program:	Aplikace přírodních věd
Obor:	Radiologická fyzika
Název práce: (česky)	Parametry ovlivňující poškození plasmidové DNA ionizujícím zářením
Název práce: (anglicky)	Parameters affecting radiation-induced plasmid DNA damage

Pokyny pro vypracování:

1. V teoretické části shrnout typy poškození DNA a principy detekce, plasmid jako modelový systém, lineární přenos energie, RBE, přehled relevantních experimentálních a výpočetních výsledků.
2. Provést experimentální stanovaní poškození DNA ozářené gama zářením Co-60 pro tři modelové plasmidy s různým počtem bázových párů, různé koncentraci plasmidu a různé vychytávací kapacitě roztoku. Experimenty musí být zopakovány nejméně dvakrát pro statistickou analýzu dat.
3. Vyhodnotit data z elektroforézy a spočítat výtěžky jednoduchých a dvojných zlomů DNA.
4. Srovnat data s předchozími obdobnými experimenty s Ne 400 MeV/u a Fe 500 MeV/u.
5. Analyzovat výsledky v závislosti na a) lineárním přenosu energie zdroje, b) počtu bázových párů plasmidu, c) koncentraci plasmidu, d) vychytávací kapacitě.

Doporučená literatura:

[1] GLASEL, Jay A. a Murray P. DEUTSCHER. Introduction to biophysical methods for protein and nucleic acid research. San Diego: Academic Press, c1995. ISBN 0122862309.
[2] von SONNTAG, Clemens. *Free-radical-induced DNA damage and its repair: a chemical perspective*. Berlin: Springer-Verlag, c2006. ISBN 3-540-26120-6.
[3] HUTCHINSON, Franklin. Chemical changes induced in DNA by ionizing radiation. Progress in Nucleic Acid. *Research and Moleclar Biology*. 1985. **32**. 115-154.
[4] MILLIGAN, Jamie R., Joseph A. AGUILERA a John F. WARD. Variation of single-strand break yield with scavenger concentration for plasmid DNA irradiated in aqueous solution. *Radiation Research*. 1993. **133**(2), 151-157.

Jméno a pracoviště vedoucího diplomové práce:

Ing. Kateřina Pachnerová Brabcová, Ph.D.
Akademie věd České republiky, v.v.i.
Ústav jaderné fyziky
Oddělení dozimetrie záření
Na Truhlářce 39/64
180 00 Praha 8

Jméno a pracoviště konzultanta diplomové práce:

Ing. Anna Michaelidesová, Ph.D.
České vysoké učení technické v Praze
Fakulta jaderná a fyzikálně inženýrská
Katedra dozimetrie a aplikace ionizujícího záření
Břehová 78/7
115 19 Praha 1

Datum zadání diplomové práce: 25. 10. 2018

Termín odevzdání diplomové práce: 6. 5. 2019

Doba platnosti zadání je dva roky od data zadání.

.....	.....	.....
garant oboru	*vedoucí katedry*	*děkan*

V Praze dne 25.10.2018

ČESKÉ VYSOKÉ UČENÍ TECHNICKÉ V PRAZE
Fakulta jaderná a fyzikálně inženýrská
-1-

Prohlášení

Prohlašuji, že jsem svoji diplomovou práci vypracovala samostatně a použila jsem pouze podklady uvedené v přiloženém seznamu.

V Praze .....

.....
Bc. Zuzana Jamborová

Acknowledgements

I would like to express my gratitude to Ing. Kateřina Pachnerová Brabcová, Ph.D. for her highly valuable guidance and patience. Furthermore, I would like to thank Ing. Anna Michaelidesová, Ph.D. for her useful and constructive suggestions regarding laboratory work and to Ing. Václav Štěpán, Ph.D. and Ing. Martin Šefl, Ph.D. who have kindly contributed with their simulation results.

This work was supported by the Czech Science Foundation, project no. 17 - 03403Y. We express our thanks to the staff of HIMAC, Japan.

Bc. Zuzana Jamborová

Název práce: Parametry ovlivňující poškození plasmidové DNA ionizujícím zářením

Autor: Bc. Zuzana Jamborová

Obor: Radiological Physics

Druh práce: Diplomová Práce

Vedoucí práce: Ing. Kateřina Pachnerová Brabcová, Ph.D., ODZ ÚJF AV ČR, v.v.i.

Konzultant: Ing. Anna Michaelidesová, Ph.D., ODZ ÚJF AV ČR, v.v.i.

Abstrakt: Přestože jsou škodlivé účinky ionizujícího záření na živý organizmus známé téměř od objevu paprsků X, stále nejsou detailně prostudovány mechanizmy radiačního poškození způsobeného těžkými nabitými částicemi vyskytujícími se přirozeně ve vesmíru nebo používanými v radioterapii. Tato práce se zaměřuje na studium výtěžků jednoduchých (SSB - single strand breaks) a dvojných (DSB - double strand breaks) zlomů na dvoušroubovici plasmidové DNA ozářené zářením ^{60}Co, urychlenými těžkými ionty neonu s energií 400 MeV/u a železa s energií 500 MeV/u. Plasmid DNA může sloužit jako zjednodušený model buňky bez přítomnosti reparačních procesů, které by se odehrávaly v živém organismu. Výsledky byly sledovány v závislosti na různé koncentraci a délce plasmidů, různé koncentraci vychytávače hydroxylových radikálů Tris (2-amino-2-hydroxymethyl-propan-1,3-diol) a různých hodnotách lineárního přenosu energie.

Klíčová slova: lokální vícečetné DNA poškození, těžké ionty, vychytávač, délka plasmidů, koncentrace plasmidů

Title: Parameters affecting radiation-induced plasmid DNA damage

Author: Bc. Zuzana Jamborová

Abstract: Even though the harmful effects of ionizing radiation on a living organism are known almost since the discovery of X rays, little is known about the radiation damage mechanism caused by heavy charged particles occurring naturally in space or used for radiotherapy. This work focuses on the study of single strand break (SSB) and double strand break (DSB) yields on the double helix plasmid DNA irradiated with ^{60}Co radiation and accelerated heavy Ne ions with energy of 400 MeV/u and Fe ions with energy of 500 MeV/u. Plasmid DNA can serve as a simplified model of a cell without the presence of repair mechanisms which would take place in a living organism. Results were obtained using different length and concentration of plasmids, different concentration of the hydroxyl radical scavenger Tris (2-amino-2-hydroxymethyl-propan-1,3-diol), and various values of linear energy transfer.

Key words: cluster damage, heavy ions, scavengers, plasmid length, plasmid concentration

Contents

1 Introduction **11**

1.1 Radiation damage of DNA 12

1.1.1 Stages of radiation damage 12

1.1.2 Direct and indirect effect, radiation chemistry of water 13

1.1.3 Types of DNA damage 15

1.2 Linear energy transfer and relative biological effectiveness 17

1.3 Plasmid as a model system 21

1.4 Densely ionizing radiation 23

1.5 Related work 24

2 Materials and Methods **25**

2.1 Gel electrophoresis 26

2.2 Plasmid samples 27

2.3 Irradiation 30

2.4 Agarose gel electrophoresis 31

2.5 SSB and DSB yield calculation 32

3 Results **34**

3.1 Optimalization 34

3.2 DNA damage yields 37

3.2.1 DNA damage yield for ^{60}Co 38

3.2.2 DNA damage yield for heavy ions 38

4 Discussion **44**
4.1 Influence of various plasmid concentrations 44
4.2 Influence of various scavenger concentrations 47
4.2.1 Result comparison 54
4.3 Influence of plasmid length 55
4.4 LET dependence 55
4.4.1 Result comparison 56
4.5 Uncertainty analysis 56

5 Conclusions **61**

Bibliography **63**

Chapter 1

Introduction

The discovery of X-rays by W.C. Roentgen in 1895 moved the scientific world. Many scholars began experimenting with this new kind of radiation, including T. A. Edison who already was a respected inventor at that time. While working with a simple fluoroscope, which was basically an X-ray source with a fluorescent screen, he soon noticed that his assistant was affected poisonously by the X-rays and concluded that "... it would not be a very popular kind of light... " and dropped further exploration in this field. Edison was not the only one noticing malign effects of ionizing radiation to a human organism, but unfortunately the knowledge of the biological effects was left unexplored until several decades later. Radiation biology and biophysics only got serious attention after the World War II (Alpen 1998). Since then, these fields have been making considerable progress as the uses of X-rays and other ionizing radiation sources have proliferated and our understanding of biological effects has greatly improved. However, the field of radiation damage caused by heavy charged particles naturally occurring in space or used in radiation therapy is still not completely understood and needs further attention.

The theoretical part of this work focuses on the basic processes of radiation damage of DNA and principles of its detection and describes plasmids as a model system for these phenomena, it explains the concepts of linear energy transfer and relative biological effectiveness. The theoretical part finishes with a brief review of relevant experimental and model results relevant to this topic.

The practical part concentrates on experimentally determining radiation damage induced by gamma rays ^{60}Co for three model plasmids with

a different number of base pairs, plasmid concentration and scavenging capacity of the plasmid solution. For statistical analysis of the data the measurements were repeated twice.

Afterwards, our experimental electrophoresis data were evaluated and the yields of single and double-strand breaks were calculated and compared to an analogical experiment we had carried out with Ne 400 MeV/u a Fe 500 MeV/u ions, as well as to previously published data describing DNA damage induced by heavy ions.

Finally we draw conclusions from how the results depend on the value of linear energy transfer, the number of base pairs of the plasmids, plasmid concentration and scavenging capacity.

1.1 Radiation damage of DNA

There is strong evidence that the biological effects of ionizing radiation are a consequence of damage caused to the most important part of each living cell, the DNA as it carries the cellular genetic information. Damage to other parts of a cell is usually swiftly compensated by synthesis of new molecules.

1.1.1 Stages of radiation damage

There are the following consecutive stages of radiation damage. The physical phase includes the actual passage of a particle with sufficient energy through a living cell, transferring its energy to the target molecule via ionization or excitations along the particle path. The physics of the energy absorption process is over in about 10^{-15} seconds. During the subsequent physicochemical stage, initial chemical products are formed. This phase ends at about 10^{-12} seconds from the impact. In the next chemical stage, the produced ions, radicals, free atoms and molecules diffuse from their point of formation and undergo chemical reactions with each other or with biological material. At about one microsecond after the original particle hit the cell, its track is no longer recognisable and all chemical reactions have already taken place. The last biological stage can take a long period of time, from hours, days, or months for cellular death, years for carcinogenesis, and generations for heritable effects (Hall and Giaccia 2006).

1.1.2 Direct and indirect effect, radiation chemistry of water

Direct and indirect effects of the ionizing radiation (IR) occur depending on the place where the absorption of radiation energy takes place. Direct effect takes place when ionizing radiation interacts directly with the target molecule (in our case DNA). Indirect effect is defined as interaction with other atoms or molecules in the cell (particularly water) which leads to the formation of free radicals, that in turn can diffuse small distances and reach the target molecule (Hall and Giaccia 2006), see Figure 1.1.

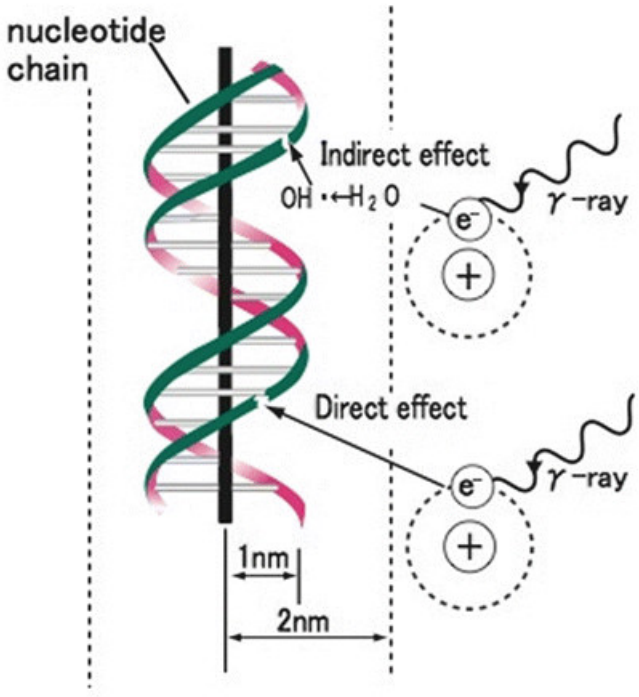

Figure 1.1: Representation of effects of ionizing radiation (IR) on DNA: direct as IR deposits energy in DNA molecule, or indirect through products of water radiolysis. The structure of DNA is shown schematically. Adapted from Hall and Giaccia (2006).

DNA damage through indirect effect is supposed to be more dominant for sparsely ionizing radiation such as X-rays. This is because unlike for densely ionizing radiation, the created radicals originate relatively far from each other and diffuse rather then recombine.

Water accounts for about 70% of a cell's weight (Alberts 2002), therefore a great part of the ionizing radiation energy is deposited in the water molecules which can subsequently be ionized (splitting into H_2O^+ and electron) or excited (H_2O^*). The immediate dissociation products

of H_2O^* are $H\cdot$ and $OH\cdot$ radicals. The ionized water molecule dissociates to $OH\cdot$ and H^+. The free electron interacts with water to produce H_2O^-, which then dissociates to $H\cdot$ and OH^-, or it reacts with water to produce a solvated electron (e_{ag}) or with hydrogen ions to produce $H\cdot$ (Alpen 1998), see Figure 1.2.

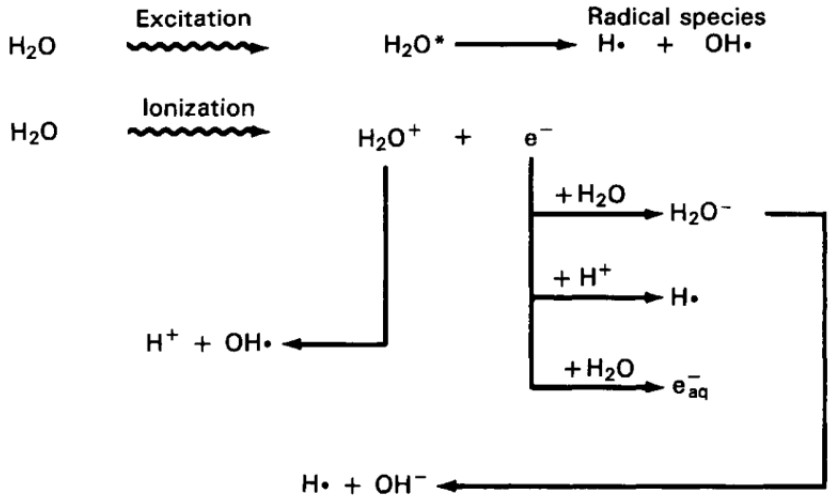

Figure 1.2: The initial products of water radiolysis (Alpen 1998).

These initial products can diffuse through the cell, interact with each other or with DNA leading to its indirect damage. These chemical reactions are complex and many reaction products are of little importance, since they do not react with DNA. The majority of the indirect damage is attributed to the very reactive hydroxyl radicals (von Sonntag 2006).

Radiation chemists use the term scavenger for the chemical species that interacts with the radicals and other active forms present in irradiated water. The scavenger, which can be any molecular species capable of interaction, reacts with the radicals to bring the water chemistry to an end. In an ideal case the scavenger reacts with all the radicals of a given type so no other chemical reactions can occur (Alpen 1998). For this reason, the presence of a scavenger lowers the level of radiation damage caused by radicals that originated during water radiolysis.

1.1.3 Types of DNA damage

A DNA molecule consists of two strands of nucleotides. A single nucleotide is made of purine and pyrimidine bases linked to a backbone which is made of an alternating sugar (deoxyribose) and phosphate group. DNA contains two purines (adenine and guanine) and two pyrimidines (cytosine and thymine). The two strands are held together by hydrogen bonds between a pair of nucleoside bases. One of the pair must be a purine and the other a pyrimidine for bonding to occur - cytosine pairs with guanine and adenosine with thymine (Watson and Crick 1953), see Figure 1.3.

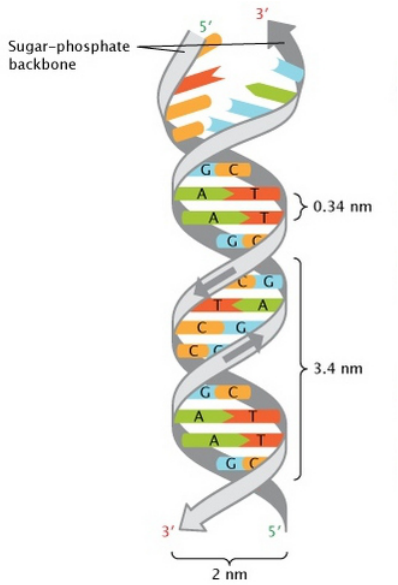

Figure 1.3: Double-helical structure of DNA. Complementary bases are held together as a pair by hydrogen bonds. The distance between two base pairs is 0.34 nm. The length of one turn of the double-helix is 3.4 nm. The width of the DNA molecule is 2 nm (Pray 2008).

Radiation or a damaging agent can damage DNA in several ways listed below (Hall and Giaccia 2006) and illustrated in Figure 1.4.

Single strand breaks (SSB) occur when one strand of the DNA molecule breaks. Both direct ionization or a free radical released by ionizing radiation can be involved in this process. SSB are one of the most common type of radiation-induced damage. Fortunately, they are easily and quickly repaired using the opposite strand as a template and therefore are of little biological consequence as far as cell killing is concerned. If the repair is incorrect, it may result in mutation.

Double strand breaks (DSB) are the most lethal form of ionizing radiation induced damage for a cell. DSB is created by the passing of a single track of ionization through both DNA strands or a pair of tracks separated only by a few base pairs. They are harder to repair as there is no template for replication like in the case of SSB. Breaks in both strands, if well separated, are repaired as independent breaks.

DNA base damage or loss takes place when the radiation induces chemical changes in nucleoside bases. Again, this is easily repairable, as the cell knows how to replace the damaged base using information from the opposite strand.

Modifications of sugar occur when the hydroxyl radical reacts with one of the hydrogen atoms in deoxyribose. If the reaction takes place on $H4'$ and $H5'$, the chemical bonds in the sugar molecule can break.

Crosslinks are newly created bonds. According to where the new chemical bond is created we differentiate intra-strand and inter-strand crosslinks. Eventually, new bonds can be created with another molecule, most likely protein, creating a DNA-protein crosslink.

Clustered lesions are a combination of the damage and breaks described above that occur within a few helical turns and are usually associated with densely ionizing radiation. These are the most critical type of DNA damage - compared to isolated damage sites, the reparation process is less effective and depends on the types of lesions and their spatial distribution as well. The unique spatial distribution of different types of DNA lesions within a cluster determines the cellular ability to repair the damage (Asaithamby, Hu, and Chen 2011). During the reparation process, the cell can produce lethal DSB while trying to repair easily repairable lesions (such as the excision of a damaged DNA base which creates another strand break close enough to a SSB that is already present in the cluster).

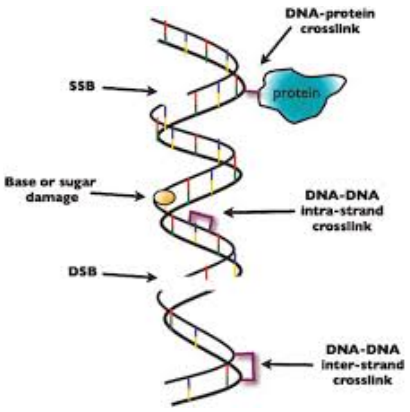

Figure 1.4: Different types of DNA damage induced by damaging agent, such as ionizing radiation (Kavanagh et al. 2013).

1.2 Linear energy transfer and relative biological effectiveness

When a charged particle moves through matter it transfers energy to it by a series of interactions (ionizations and/or excitations) occuring randomly. Linear energy transfer (LET) describes the rate at which a particle loses its energy along its track and relative biological effectiveness (RBE) describes the strength of the biological response to that particle. One can observe that the concepts of LET and RBE are linked. The next section will describe their characteristics in more detail.

In order to explain the difference between them we first have to understand how a particle loses energy in matter.

Energy deposition is a stochastic quantity that is difficult to apply in practise. Biological effect is related to the quantity of energy deposited in elemental structures of very small size as radiosensitive components occupy only a portion of the cell. As energy is not deposited homogenously in the particle track it is of interest to use microdosimetry to look at the spatial distribution of this energy deposition (Figure 1.5). Differences in microdosimetric energy deposition lead to different biologic consequences even if the total absorbed doses in a target volume may be physically equal (Lehnert 2008). An example of particle tracks caused by various radiation sources is illustrated in Figure 1.6.

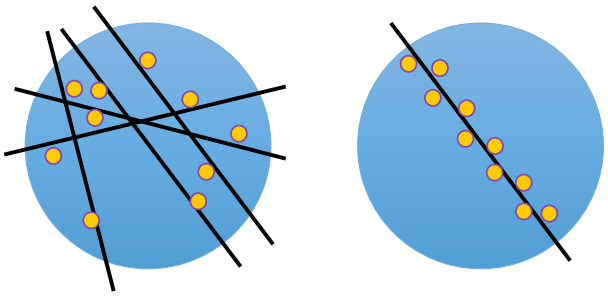

Figure 1.5: Different energy deposition for low LET radiation (on the left, energy is distributed homogeneously) and high LET radiation (on the right, the energy is distributed inhomogeneously).

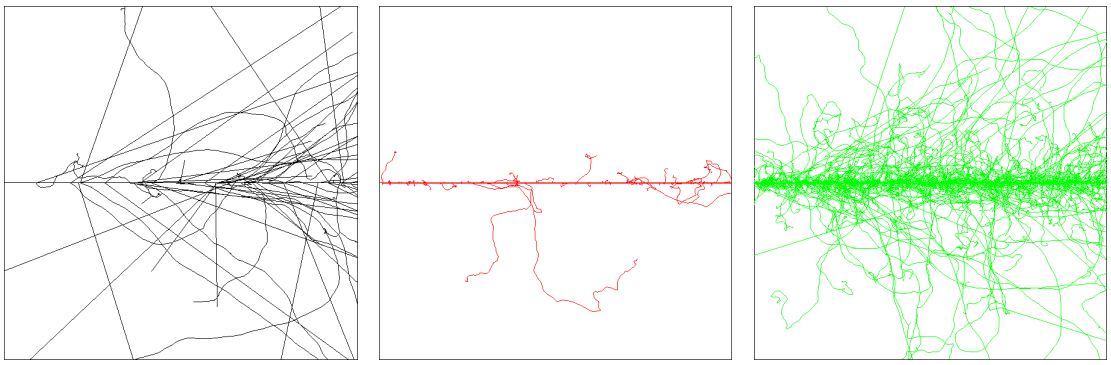

Figure 1.6: Computer simulation of particle tracks for the following radiation sources (from left to right): ^{60}Co - 5000 primary particles, 200 MeV protons - 500 primary particles and 400 MeV/u carbon ions - 50 primary particles (Pachnerová Brabcová, Štěpán, et al. 2017).

LET is a quantity representing the amount of energy transferred per unit length of the track by charged particles in a given material:

$$LET = dE/dl \tag{1.1}$$

where dE is the average energy locally imparted to the medium by a charged particle of specified energy in traversing a distance of dl. The dimension of LET being J/m, but keV/μm us used more conveniently (Hall and Giaccia 2006).

The energy loss dE along dl is also dependent on particle velocity v, its charge Z and the electron density of the target ρ:

$$dE/dl \propto (Z^2\rho)/v^2 \tag{1.2}$$

This relation implies that different particles have different values of dE/dl, therefore LET is a simplified way to describe the quality of different radiation types. Another implication is that for a given ionizing particle the rate of energy deposition in the absorbing medium increases as the particle slows down. Therefore, a beam of radiation can only be described as having an average value for LET (Lehnert 2008).

The situation is complicated by the fact that it is possible to calculate an average in different ways. The most common used methods are calculations of track average or energy average (as illustrated in Figure 1.7). Those two methods do not lead to big difference for X-rays or monoenergetic charged particles, but are significantly different for neutrons (Hall and Giaccia 2006).

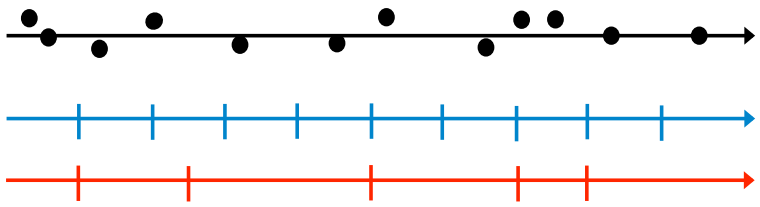

Figure 1.7: Illustration shows differences when using track average (blue line) and energy average (red line) for the same unit track length (black, line, points represent the sites of energy deposition). The track average is calculated by dividing the track into equal lengths and averaging the energy deposited in each length. The energy average is calculated by dividing the track into equal energy intervals and averaging the lengths of the track that contain this amount of energy.

RBE is used to compare two radiation beams of different LET values. It represents the ratio of the absorbed dose of a reference radiation to the absorbed dose of radiation of interest in the same target volume, each dose yielding to the same degree of biologic effect of a specific type. In comparing different radiations, it is customary to use 250 kV X-rays as the reference radiation.

As LET increases, the RBE increases slowly at first and more rapidly as LET increases beyond 10 keV/μm. It reaches a maximum at about 100 keV/μm and then falls to lower values again due to so called overkill effect (Figure 1.8). 100 keV/μm is the optimal LET (as it has the greatest RBE) because the average separation between ionizing events is similar to the diameter of DNA and double string breaks can be most efficiently produced by a single track. Ionization with LET $>$ 100 keV/μm is inefficient because more energy than necessary is deposited at the target as the ionizing events are too close together (Hall and Giaccia 2006).

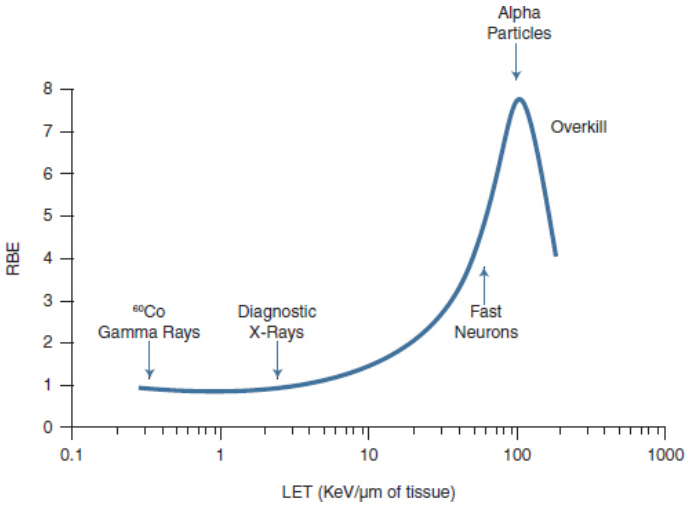

Figure 1.8: RBE as a function of LET (Medicine and Council 2014).

According to Hall and Giaccia 2006 LET is a "worse than useless" quantity, but is useful as a simple way to indicate the quality of different types of radiation.

Disadvantages include that LET is defined along the particle track and does not provide information about energy fluctuation or longitudial dispersion of the track, its value changes over the track length and has to be averaged. An average value of LET does not describe the individual energy-loss events that occur along the track of a particle which are important because they are the reason why equal doses of different radiations have different biologic effectiveness.

LET quantity has been used in the past to determine the value of the radiation quality factor (now referred to as the radiation weighting factor), which has been used to convert absorbed dose to equivalent

dose. This is acceptable for implementing radiation protection criteria for routine applications for radiation workers, but it is not sufficient for making quantitative correlations with RBE for many different biological endpoints (Takatsuji, Yoshikawa, and Saski 1999).

1.3 Plasmid as a model system

Plasmids are small, circular, double-stranded DNA molecules. They are distinct from a cellular chromosomal DNA because they do not carry any vital gene necessary for the cell and can replicate independently on main genome (Figure 1.9). They exist in bacterial cells and in some eukaryotes as well. Some plasmids can carry genes that provide bacteria with genetic advantages, such as resistance to antibiotics. They have a wide range of lengths, varying from one thousand DNA base pairs (bp) to hundreds of thousands of base pairs. Artificially produced plasmids that are used as tools to clone, transfer, and manipulate genes are called vectors in radiobiology. They are used as a simplified system to model DNA because they have the advantage of a circular structure and well defined small size compared to chromosomal DNA. The relatively small size allows simple manipulation and it is possible to analyze them with uncomplicated and cheap methods. If dissolved in water, a model of a cell without its reparation processes can be obtained.

Under the native cellular conditions, the strands of closed circular molecule are covalently linked into a higher order compact helical architecture called supercoiled; with one plasmid being able to exist in several topoisomeric conformations (Higgins and Vologodskii 2015). The degree of the interwinding and the number of interwound branches adopted by the plasmid DNA becomes more complex with decreasing salt and DNA concentration (Zhu et al. 2010).

Radiation strand breaks on circular plasmids have the following characteristics. A single strand break (SSB) causes the supercoiled plasmid to relax into open circular form, a double strand break (DSB) into linear form and consecutive DSB will cut the DNA into fragments (Figure 1.10). These forms can be separated by various methods, mentioned later in this work. If the plasmid is irradiated in dried form, the indirect effects are fully suppressed, if in liquid water, the indirect effects can be moderated by scavengers (Hutchinson 1985).

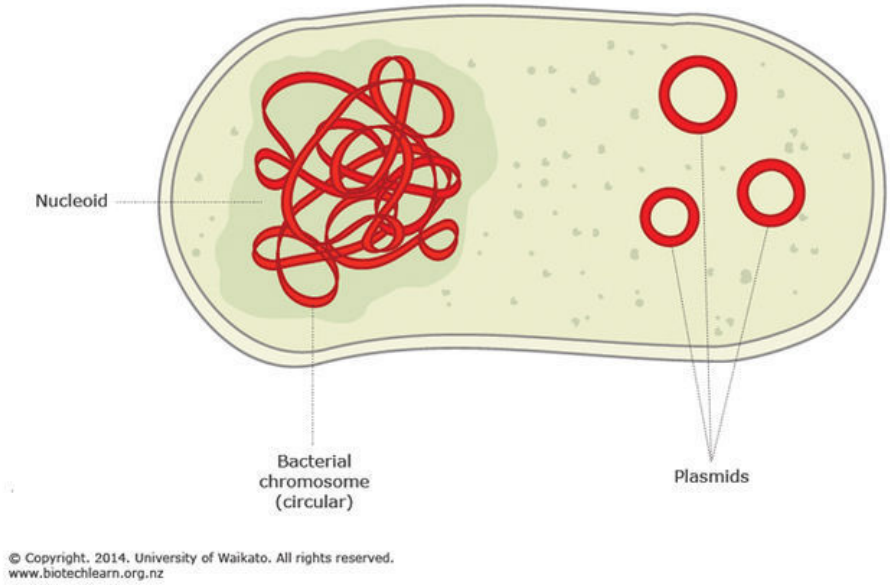

Figure 1.9: Procaryotic cell with plasmid and chromosomal DNA.

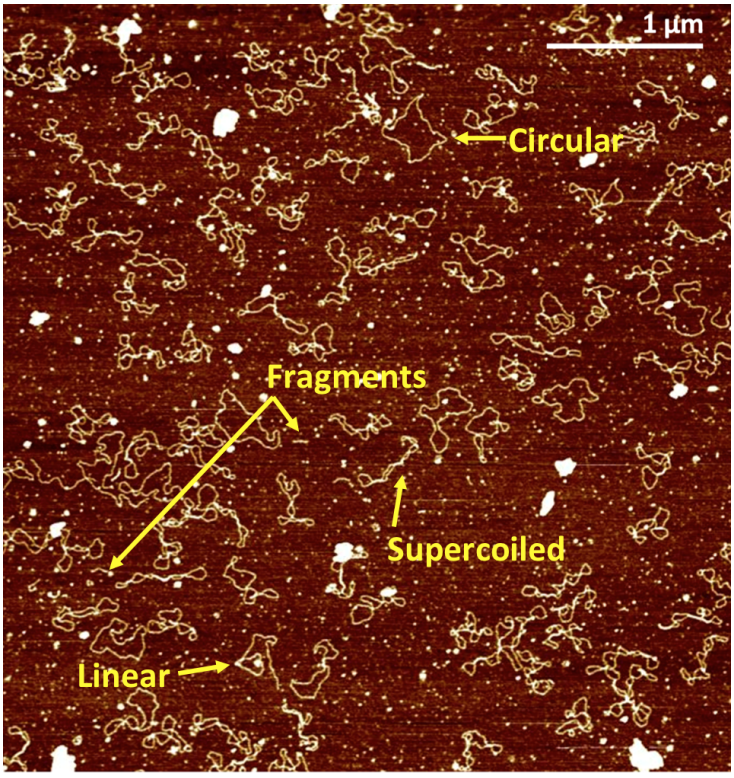

Figure 1.10: Plasmid forms of pBR322 adsorbed on mica surface as seen under an atomic force microscope (AFM). Courtesy of K. Pachnerová Brabcová.

1.4 Densely ionizing radiation

Densely ionizing radiation (DIR) are accelerated charged particles, such as protons and heavy ions - elements like carbon, neon or iron, that are positively charged because they are deprived of one or more electrons. As an accelerated charged particle passes a material, it continuously loses energy through ionizations and excitations of the atoms of the surrounding medium and the ionization density is higher than that produced by gamma or X. DNA damage depends on radiation quality and with growing ionization density the damage becomes clustered and therefore more difficult to repair.

Charged particles of high energy are encountered in space and are a major health hazard for future human missions exploring Mars or generally flights beyond the protection of the Earth's magnetic shielding. Commonly the space environment is categorized into three sources of ionizing radiation, each of which is associated with different energy and prevalence. Galactic cosmic rays originate outside the Solar System and contain approximatlly 87% of fast moving hydrogen ions (protons) 12% helium ions (alpha particles) and 1–2% of other high energy nuclei. Solar particles emitted by the Sun during solar flares consist primarily of protons with kinetic energies up to several GeV. Finally, solar wind consist of mostly low energy protons and electrons. Their dose rates vary with the solar cycle (Chancellor et al. 2018).

Exposure to high energy proton radiation occurs during commercial flights as a consequence of secondary galactic cosmic radiation. The level of exposure depends on the flight altitude and duration and is significantly increased during a solar storm.

The use of the charged particles in radiotherapy (currently carbon ion or proton therapy) is increasing as well. Compared to conventional X ray or gamma therapy ion therapy allows targeted dose deposition in tumours and is reducing the dose in surrounding healthy tissues. During the last decade, 63 particle therapy treatment centres were opened worldwide, with another 29 planning to start treatment by the year 2020 (information as of April 2019, *PRCOG* 2019). This is another imperative reason that we gain a deeper understanding of the biological effects associated with exposure to DIR.

1.5 Related work

Radiation induced nuclear foci is a technique used to visualise DNA damage on cells through the recruitment of DNA repair proteins to sites of DNA damage (Hall and Giaccia 2006). The detection is based on the quantification of DNA damage response proteins of the histone group, H2AX. The phosphorylated H2AX, called gamma-H2AX, forms subnuclear foci, which can be located and scored with fluorescent microscope after an immuno-fluorescent staining with antibody anti-gamma-H2AX (Celeste et al. 2003). If the value of the foci is measured over time it reflects the kinetics of repair.

Of course, this reparation mechanism does not take place in plasmids. The relationship between DSBs in plasmids and DSBs in cells is not straightforward, nevertheless double string breaks indicate the level of primary damage in plasmids which is nearly impossible to measure in cells due to rapid reparations.

Simulations show that generally, with increasing LET, less DNA strand breaks are formed per unit dose in a cell. Individual strand breaks tend to aggregate as DSB, whose yields increase with LET up to a saturation level (at around 300 keV/μm) when the increasing formation of DSB clusters is counterbalanced by a strong decrease in isolated DSBs and above 500 keV/μm even the number of DSB clusters decreases with increasing LET. This is remarkably similar to patterns known from cell survival studies, LET-dependencies with pronounced maxima around 100–200 keV/μm occur on nanometre scale for sites that contain one or more DSBs, and on micrometre scale for megabasepair-sized DNA fragments (Friedland et al. 2017).

Measurements of clustered damages are a subject of intensive research over the last three decades. Experimental results, however, show significant deviations from theoretical data. Most experimental studies reported either a relatively weak or no dependence of the DSB yield on LET, depending on the method used (Leloup et al. 2004). For an overview, see works of Terato et al. 2014 and A. G. Georgakilas, O'Neill, and Stewart 2013.

Chapter 2

Materials and Methods

There are multiple methods to study radiation damage of nucleic acids and proteins such as ion chromatography, mass spectroscopy, microscopic methods (AFM - atomic force microscopy), or electrophoresis. The last one is the highest resolution method available for separation of proteins and nucleic acids or their fragments. It is the ideal method to study radiation damage of DNA as it allows separation of intact and damaged plasmids by their size or conformation (Glasel and Deutscher 1995).

The basic idea of electrophoretic method is very simple. It uses the movement of a charged particle in an externally applied electric field. A molecule of charge q in an electric field E is experiencing an electric force

$$F = qE \tag{2.1}$$

Opposing the electrical force E there is frictional force. In a free environment, the frictional force is linearly proportional to the velocity v of the molecule. The frictional coefficient f reflects the size and shape of the molecule. Under this two opposing forces the molecule will reach a steady state when it is moving with a constant velocity and the two forces equal

$$qE = fv \tag{2.2}$$

The electrophoretic mobility μ is defined as the steady state velocity per unit field and is the characteristic property describing the response of the molecule to electric fields.

$$\mu = v/E = q/f \tag{2.3}$$

2.1 Gel electrophoresis

One can choose from variations of electrophoresis techniques depending on the measured size of the molecules, their charge or required accuracy. Most of them are relatively inexpensive and easy to perform. Agarose (a polysaccharide extracted from seaweed) or polyacrylamide is used for electrophoresis gel preparation. Polyacrylamide gels are run in a vertical configuration, agarose gels are typically run horizontally. Starch gel electrophoresis is more of a historic relict today. Separation of large molecules (more than 20 kbp) can no longer be achieved with direct electric field, therefore alternating field is employed in so called pulsed electrophoresis. With each reorientation of the electric field, smaller sized DNA will begin moving in the new direction more quickly than larger DNA. Capillary gel electrophoresis has the advantage of a short analysis time, high degree of reproducibility combined with a good resolving power for detection of DNA fragments. Atomic force microscopy has been developed to a stage that double strand breaks and the length of the resulting fragments can be detected (von Sonntag 2006).

Protein electrophoresis is a bit more complicated, because unlike DNA, proteins do not have only negative electric charge. Methods used include 2D electrophoresis, SDS gel electrophoresis or isoelectric focusing (Glasel and Deutscher 1995).

Gel electrophoresis is the most widely used electrophoresis technique. The gel and the method is selected according to the length of the DNA fragments that are to be separated. Agarose gel serves as a medium to separate fragments of lengths between 100 bp to 25 kbp. For smaller fragments polyacrylamide gels are used and for extremely long fragments pulse field electrophoresis is the best choice (Lee et al. 2012).

An important factor that affects the molecule mobility is the density of the gel medium as it determines the size of pores through which the DNA molecules travel. The denser the gel, the slower the separation. A dense gel is therefore suitable for separation of smaller fragments.

The voltage used to create the electric field should not be too high, because the produced heat would lead to gel deformation. On the other hand, if the voltage is low, the rate of DNA separation is slow and the molecules tend to diffuse to the surroundings. Both extremes lead to blurred or deformed lines in the gel. The specific voltage has to be

chosen depending on the size of the apparatus and general circumstances of the experiment.

Another factor that affects mobility is the selection of buffer system. Buffers provide ions necessary for electric conductivity and they keep the pH in desired range. A typical buffer system used in agarose gels is TAE (Tris-Acetate-EDTA with EDTA being short form of Ethylendiaminetetraacetic acid). Usually the same buffer is used in the gel and electrode reservoirs. Another common buffer is TBE (Tris-Borate-EDTA).

DNA samples are loaded into the wells created in the gel, usually in the presence of a loading dye. The dye adds colour and density to the DNA sample causing it to sink into the gel and allowing to place the sample more precisely and to visually control the progress of the sample in a gel.

In order to estimate the sizes of the samples, their movement is compared to a set of standards of a DNA ladder (a mix of linear DNA) which indicates how far molecules of known sizes migrate in the electric field.

To be able to see the distance travelled by separate plasmid forms a fluorescent dye that binds to the DNA has to be added. It can be mixed into the gel before it is poured to a mould and left to dry. The results show as bright bands when placed under an UV lamp.

2.2 Plasmid samples

For this experiment, we worked with three plasmids of different length provided by New England Biolabs Inc. The plasmids were selected so that the next one is approximately double in size than the previous. The original plasmid concentration of all three samples given by the manufacturer was 1000 μg/ml supplied in 1 $\times$ TE solution (10 mM Tris-HCl, 1 mM EDTA, pH 8.0). The used plasmids follows together with a simulated illustration of their supercoiled conformations on Figure 2.1:

- **pUC19** consisting of 2686 base pairs. Originally isolated from *E. coli*, pUC19 is one of a series of plasmid cloning vectors created by Joachim Messing and co-workers. The designation "pUC" is derived from the classical "p" prefix (stands for "plasmid") and the

abbreviation for the University of California, where early work on the plasmid series had been conducted.

- **pBR322** consisting of 4361 base pairs. Is a widely used *E. coli* vector. Created in 1977 in the laboratory of Herbert Boyer at the University of California, San Francisco, it was named after the post-doctoral researchers who constructed it - BR stands for "Bolivar" and "Rodriguez."

- **pKLAC2** consisting of 9107 base pairs. Originating from Kluyveromyces lactis, its name comes from the ability to assimilate lactose and convert it into lactic acid.

However, when we re-measured the plasmid concentrations, the manufacture estimation of 1000 μg/ml turned out to be overrated. We measured the optical density of the samples at 260 nm (OD_{260}) spectrophotometrically and by knowing that when OD_{260} equals 1 then the measured double strand DNA solution contains 50 ng/μl of DNA, sample concentrations were calculated as an average of three measurements. Results are summarized in Table 2.1.

Table 2.1: DNA sample concentrations as estimated spectrophotometrically.

Plasmid sample	pUC19	pBR322	pKLAC2
Measured concentration [ng/μl]	590	466.7	840

There is a certain number of damaged molecules even in a non irradiated plasmid that have formed during sample preparation and storage. Gel electrophoresis revealed that pUC19 and pBR322 samples contained both over 95% of supercoiled form prior to irradiation, pKLAC2 was already damaged with only 50% supercoiled form before the irradiation. Therefore for the last set of experiments with ^{60}Co we have prepared our own pKLAC2 plasmid by inoculating liquid *E. coli* culture, grown in Lysogeny Broth (LB) medium. The measured concentration of this plasmid sample is in Table 2.2.

Table 2.2: "Homemade" pKLAC2 sample concentration as estimated spectrophotometrically.

Plasmid sample	pKLAC2
Measured concentration [ng/μl]	106

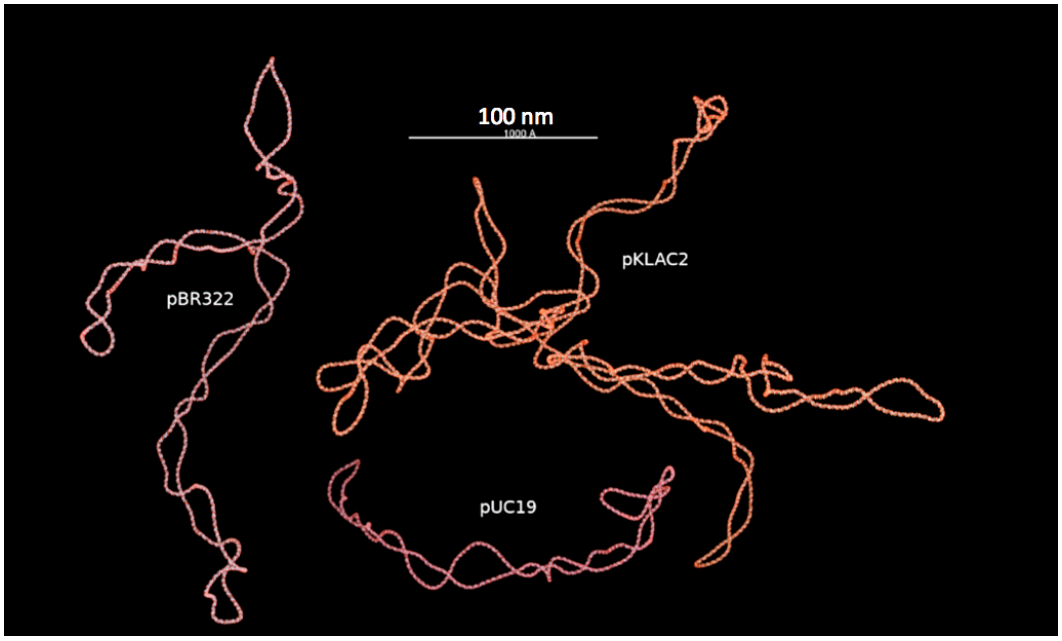

Figure 2.1: Computer model of our three plasmid samples. Courtesy of Václav Štěpán and Martin Šefl.

The samples were diluted to concentrations of 10 ng/μl, respectively 50 ng/μl with deionized water. Potassium phosphate buffer, pH 7, was added to reach 20 mM.

Hydroxyl radical scavenger Tris (2-amino-2-(hydroxymethyl) propane-1.3-diol) was added to a part of the samples, allowing us to study damage yields under various scavenging conditions given by scavenger capacities. Scavenging capacity is defined as the characteristic reaction rate of a radical with a scavenger and equals $k \times [S]$ where k is a rate constant and $[S]$ scavenger concentration. The rate constant for reaction of Tris and hydroxyl radical is 1.5 $\times$ 109 M/s (Hodgkins, Fairman, and O'Neill 1996).

The concentrations of Tris used to modify the scavenging capacity of the plasmid solutions are summarised in Table 2.3. Scavenging capacity 4.2×10^5 s^{-1} is determined only by the residual concentration of TE buffer solution, no additional Tris was added. Scavenging capacity 10^8 s^{-1} corresponds to cellular scavenging conditions (Klimczak et al. 2009).

After this preparation, the samples were ready for the irradiation. Prior to the application of the irradiated samples on the electrophoresis gel 2 μl of DNA Loading Dye (provided by Thermo Scientific) was added

Table 2.3: Scavenger concentrations used in our samples with scavenging capacity of the solution.

Scavenger concentration [M]	**Scavenging capacity [s^{-1}]**
2.8×10^{-4}	4.2×10^{5}
6.7×10^{-3}	1.0×10^{7}
6.7×10^{-2}	1.0×10^{8}

to them. It contains two different dyes (bromophenol blue and xylene cyanol FF) for visual tracking of DNA migration during electrophoresis. The presence of glycerol in the dye ensures that the DNA in the ladder and sample forms a layer at the bottom of the well.

2.3 Irradiation

For our experiment the plasmid samples (prepared as per 2.2) were irradiated by three different radiation sources. Gamma irradiation was used to optimize gel electrophoresis conditions prior to the respective measurements, which were carried out with plasmids damaged by ^{60}Co, 400 MeV/u Ne and 500 MeV/u Fe ions. The samples were kept in below zero temperatures before and after the irradiation.

- Gamma irradiation

  Sample irradiation with ^{60}Co source was performed at Department of Radiation Dosimetry in Prague, Czech Republic. LET value of ^{60}Co gamma rays is about 0.3 keV/μm and the delivered doses were up to 100 Gy. For irradiation at different doses either 10 μl (for plasmid sample concentration of 10 ng/μl) or 2 μl (for plasmid sample concentration of 50 ng/μl) of sample volume was pipetted into several standard polypropylene tubes of 1 ml volume.

- Heavy ion irradiation

  Other set of plasmid samples was irradiated with 500 MeV/u iron (LET 197.6 keV/μm) and 400 MeV/u Ne ions (LET 30.4 keV/μm) at the Heavy Ion Medical Accelerator in Chiba (HIMAC), National Institute of Radiological Sciences, Japan. The samples were irradiated in polypropylene microtubes of total volume 0.7 ml (Figure 2.2) and doses from 1 to 100 Gy were delivered. A control sample

of all three plasmids stayed in the Czech Republic and was later used as the non irradiated zero dose reference.

Figure 2.2: Microtubes containing plasmid samples prepared for the irradiation on HIMAC.

2.4 Agarose gel electrophoresis

All irradiated samples were analysed using agarose gel electrophoresis (AGE). The density of agarose gel is expressed in percentage, that means for a 1% gel 1 g of agarose powder dissolved in 100 ml buffer (0.5 × TAE) is used. The mixture is heated to a high temperature until all the agarose powder has melted and then poured into a mould where a comb is placed to the top part of it to make wells where the samples will be pipetted. We used a comb that created wells of approximately 15 μl volume.

Once the gel has thickened, it acts like a sieve for the DNA molecules. The greater the agarose concentration, the smaller the pores created in the gel and the more difficult is it for larger molecules to move through it. The gel was then placed into a tank filled with 0.5 × TAE buffer and run under a constant voltage of 100 V for about 70 or 120 minutes depending on the particular experiment (see Figure 2.3). Gels were stained with fluorescent dye SYBR Green (it binds to double-stranded DNA molecules by intercalating between the DNA bases; provided by Sigma Aldrich) in

a concentration of 1μl to 100 ml and imagined under UV light on a transilluminator table. The acquired images showing bright molecule bands were processed using an in-house developed software named Luthien for integrating the peaks corresponding to supercoiled, circular and linear plasmid form.

We tested various concentrations of agarose gels in order to estimate which performs best for each plasmid. Selection criteria were for all three of the forms to separate fully and the resulting bands to be well defined.

Figure 2.3: Agarose gel electrophoresis horizontal apparatus used in this study. The gel is placed in the buffer filled tank and electrical field is applied. The blue lines indicate the position of the migrating molecules.

2.5 SSB and DSB yield calculation

For calculation of DNA damage yields we have used the model of Cowan et al. describing the transitions between supercoiled (S), circular (C) and linear (L) DNA forms as well as fragments (F) as a consequence of exposition to cutting enzymes that can produce strand breaks in DNA. The enzyme "nicks" each of the single strands at random sites and times. A nick breaks the bonds in the sugar-phosphate chain and separates two successive bases on one strand of the DNA molecule. The first nick lets

the supercoiled form relax, subsequent nicks increase the probability that two of them are sufficiently close to break the molecule which loses its circular structure. Continued exposure to the enzyme will cause other DSB and eventually the molecule becomes fragmented. The nature of this breaks is equivalent to breaks created by radiation (Cowan, Collis, and Grigg 1987).

The model provides mathematical equations for the proportions of DNA molecules for each of the four plasmid forms after receiving a known dose (D) and calculates μ and ϕ (yields of SSB and DSB per plasmid per Gy). The authors also considered the situation where not 100 % of the non irradiated material is in supercoiled form, but instead a mixture of forms (μ_0 and ϕ_0).

The theory can by simplified when an independent enzyme creating DSB directly is added and assuming that this mechanism dominates in the formation of linear and fragmented molecules, so just one "cut" is sufficient for creating a linear form and two for fragmentation. SSB accumulation leading to DSB can be neglected, the only effect of nicking is the creation of circular form from the supercoiled.

The derived equations are following:

$$S(D) = e^{-(\mu_0+\mu D)}e^{-(\phi_0+\phi D)} \tag{2.4}$$

$$L(D) = (\phi_0+\phi D)e^{-(\phi_0+\phi D)} \tag{2.5}$$

$$C(D) = (1-e^{-(\mu_0+\mu D)})e^{-(\phi_0+\phi D)} \tag{2.6}$$

$$F(D) = 1-e^{-(\phi_0+\phi D)}(1+\phi_0+\phi D) \tag{2.7}$$

Since the fragments are usually not detected using agarose gel electrophoresis, the equations (2.4 - 2.6) can be divided by $1-F(D)$ and we get the relative proportions of supercoiled, linear and circular form among the non - fragmented forms.

$$S'(D) = e^{-(\mu_0+\mu D)}/(1+\phi_0+\phi D) \tag{2.8}$$

$$L'(D) = (\phi_0+\phi D)/(1+\phi_0+\phi D) \tag{2.9}$$

$$C'(D) = (1-e^{-(\mu_0+\mu D)})/(1+\phi_0+\phi D) \tag{2.10}$$

Model parameters were calculated using MATLAB R2017a (MathWorks, Inc.) and measured data were fitted to the model.

Chapter 3

Results

3.1 Optimalization

In order to estimate the optimum gel percentage for each of our three plasmid samples we have prepared 0.8%, 1%, 1.1%, 1.2% and 1.3% gels. Onto each of the gels we applied the samples of three plasmids irradiated with various doses; the first and the last well contained DNA ladder. The DNA ladder was provided by New England BioLabs Inc. and had a size range of 10 kbp to 80 bp.

Figure 3.1 shows gel concentration of 1.3% with applied samples. The area marked with a red rectangle contains our largest plasmid sample pKLAC2. Comparing to the same sample applied to 0.8% gel (Figure 3.2) we can see that the bands are not as clearly defined, therefore the lower concentration is more suitable for this length of plasmid. We have made analogical comparisons for the other used plasmids (pBR322 and pUC19).

We have also compared the visual quality of plasmid bands for two gels of the same percentage but a different total volume. We prepared a thinner and thicker gel (100 ml vs 120 ml on 1% agarose gel concentration) and concluded that the thinner gel works slightly better for our experiment. The difference is not overwhelming (Figure 3.3), but if cost minimalisation is taken into account as another decision criterion, a smaller volume of gel is preferred.

For subsequent measurements we have chosen 0.8% gel for our largest sample pKLAC2, 1% gel for pBR322 and 1.2% gel for the smallest plasmid sample pUC19 and a gel volume of 40 or 100 ml.

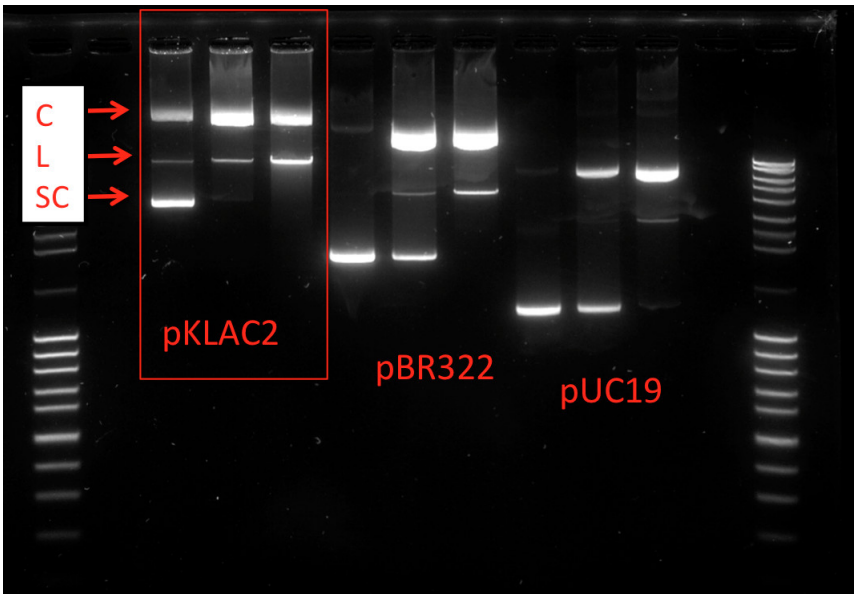

Figure 3.1: Optimization of electrophoretic separation for plasmids DNA of different length on an agarose gel with concentration of 1.3%. The three electrophoretically separated plasmid forms - supercoiled (SC), circular (C) and linear (L) - are illustrated for the pKLAC2 sample.

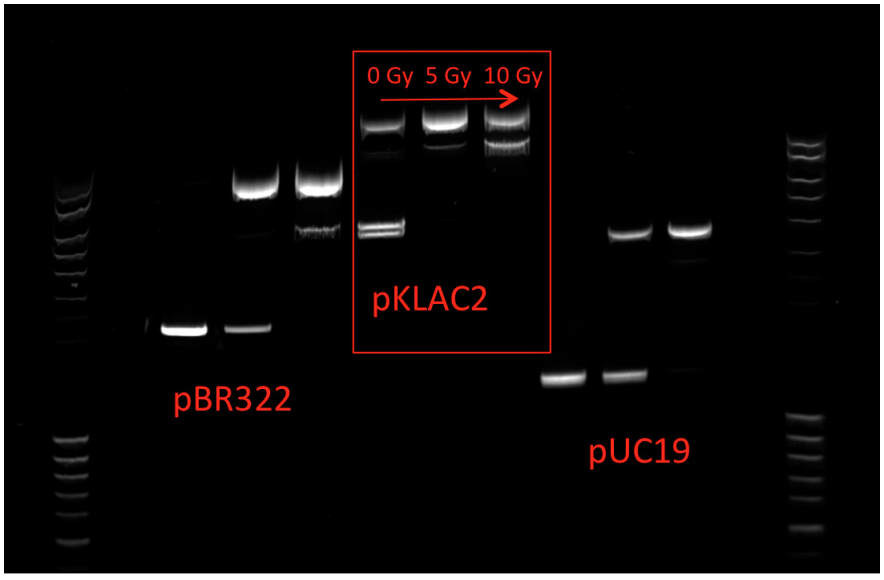

Figure 3.2: Optimization of electrophoretic separation for plasmids DNA of different length on an agarose gel with concentration of 0.8%. Irradiation doses of pKLAC2 sample are marked in the picture for illustration.

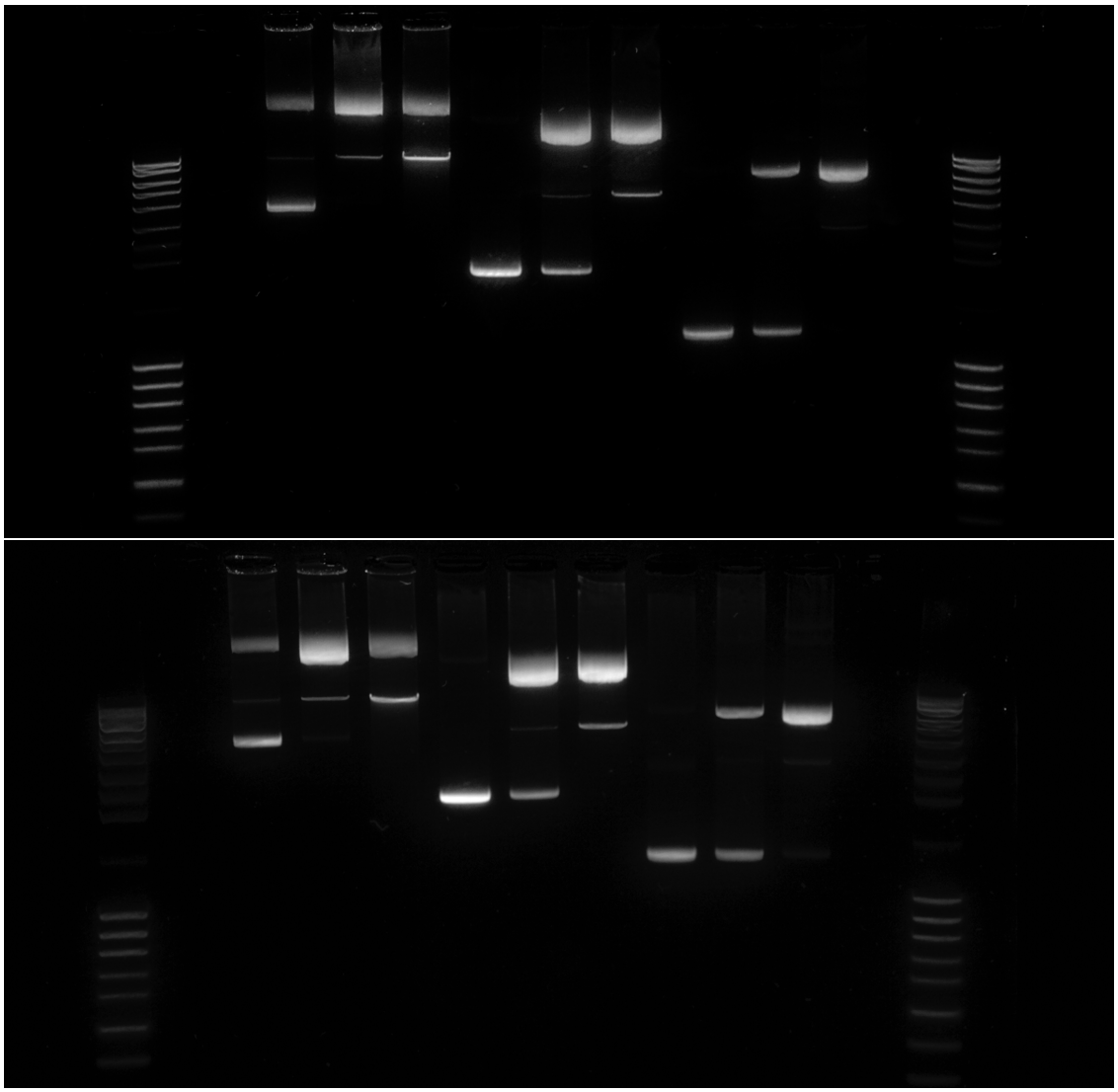

Figure 3.3: Optimalization of gel volume for further experiments. Visualised samples on 1.3% gel. Figure on top is of an 100 ml gel, bottom of an 120 ml gel.

3.2 DNA damage yields

The irradiated samples were analysed by agarose gel electrophoresis (as described in section 2.4) using the gel concentrations determined earlier in this chapter. The obtained images were saved in 8 bit resolution and processed with the in-house tool Luthien. Luthien was used to integrate intensity peaks corresponding to the three plasmid forms in the image spectrum (Figure 3.4).

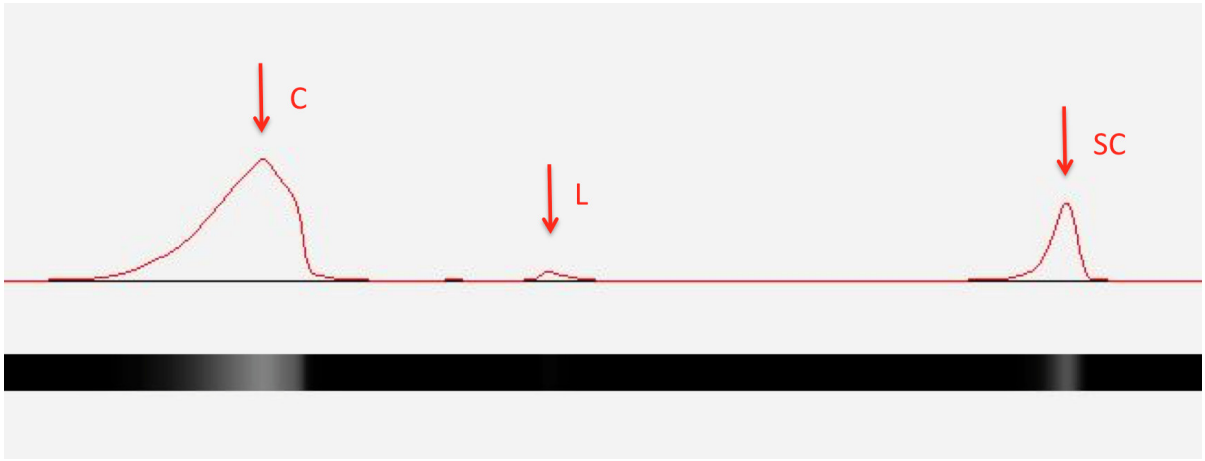

Figure 3.4: Peaks representing the circular (C), linear (L) and supercoiled (SC) plasmid forms in a spectrum figured by Luthien software.

Relative amounts of DNA in each of the three plasmid conformations (S', C' and L') were calculated for each dose using the results from Luthien programme.

$$S' = I_S/I_T \tag{3.1}$$

$$L' = I_L/I_T \tag{3.2}$$

$$C' = I_C/I_T \tag{3.3}$$

$$I_T = I_S + I_L + I_C \tag{3.4}$$

Where I_S, I_L, I_C are the integrated intensities of each form and I_T the total integrated intensity. The relative values were used as the input for fitting the data to the Cowan model described in Chapter 2.5.

3.2.1 DNA damage yield for ^{60}Co

Cowan model was fitted to the relative fractions of supercoiled, circular (referred to as "relaxed" in some literature) and linear forms obtained by integration of measured spectra. Examples of experimental data fitted to the model for pBR322 plasmid for different plasmid concentrations are in Figure 3.5.

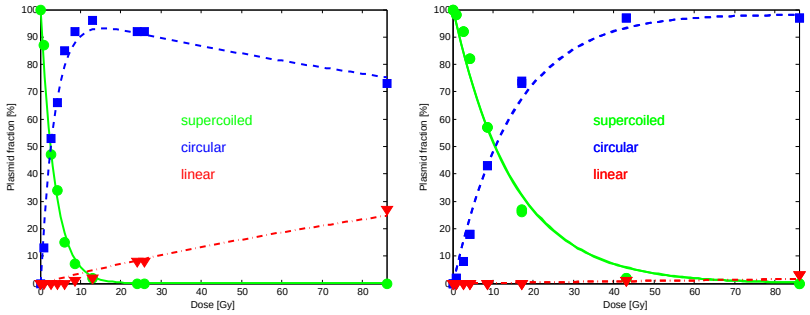

Figure 3.5: Relative yields of supercoiled, circular and linear form for pBR322 plasmid sample after ^{60}Co irradiation without an added scavenger. Plasmid concentration 10 ng/μl shown on the left, 50 ng/μl on the right.

Table 3.1 sumarizes SSB and DSB damage yields per length unit and dose (referred to as G(SSB) and G(DSB) respectively) which were calculated by dividing the parameters μ and ϕ obtained from the model by Cowan et. al. by the length of the plasmid DNA in base pairs.

3.2.2 DNA damage yield for heavy ions

Upon receiving the irradiated samples back at our laboratory from Japan they were analysed employing AGE method. We obtained 40 gel electrophoresis images of DNA for further analysis. Figure 3.6 shows a typical agarose gel with electrophoretically separated plasmid forms for 0–100 Gy plasmid irradiation by 500 MeV/u Fe ions without the presence of radical scavengers. Examples of experimental data fitted to the Cowan model for pUC19 plasmid in samples with three scavenging capacities are shown in Figure 3.7.

G(SSB) and G(DSB) were calculated by dividing the parameters μ and ϕ obtained using the model by Cowan et. al. by the length of the plasmid DNA in bp.

Table 3.1: Radiation-induced yields of SSB and DSB per 10^6 base pairs and Gy after ^{60}Co irradiation for all three studied plasmids under different scavenging conditions in two plasmid concentrations. Missing values for pKLAC2 are due to an error in the electrophoresis apparatus settings during the measurement of this sample.

Plasmid, Concentration	**Scavenging capacity (s^{-1})**	**G (SSB) [Mbp^{-1} Gy^{-1}]**	**G (DSB) [Mbp^{-1} Gy^{-1}]**
pUC19, 10 ng/μl	4.2×10^5	60.915	1.1088
	1.0×10^7	6.896	0.1975
	1.0×10^8	0.624	0.0023
pBR322, 10 ng/μl	4.2×10^5	63.334	0.8714
	1.0×10^7	6.673	0.0295
	1.0×10^8	0.825	0.0013
pKLAC2, 10 ng/μl	4.2×10^5	18.354	0.7394
	1.0×10^7	-	-
	1.0×10^8	1.261	0.0001
pUC19, 50 ng/μl	4.2×10^5	8.534	0.0001
	1.0×10^7	1.178	0.0001
	1.0×10^8	0.188	0.0010
pBR322, 50 ng/μl	4.2×10^5	15.157	0.0445
	1.0×10^7	3.646	0.0001
	1.0×10^8	0.413	0.0006
pKLAC2, 50 ng/μl	4.2×10^5	14.209	0.0001
	1.0×10^7	4.085	0.0000
	1.0×10^8	0.494	0.0019

Results for 500 MeV/u Fe irradiation are summarised in Table 3.2, Table 3.3 contains the yields for 400 MeV/u Ne irradiation.

Due to limitations on available beam time at HIMAC and a large number of samples to be analyzed, the experiments were not repeated and a variation of the samples could not be estimated. However, we can assume that the relative standard deviation will be similar as in analogical studies, where it was estimated to 15% (Pachnerová Brabcová, Sihver, et al. 2014).

Table 3.2: Radiation-induced yields of SSB and DSB per 10^6 base pairs and Gy after 500 Me/u Fe ions irradiation for all three studied plasmids under different scavenging conditions and both used sample concentrations.

Plasmid, Concentration	**Scavenging capacity (s^{-1})**	**G (SSB) [Mbp^{-1} Gy^{-1}]**	**G (DSB) [Mbp^{-1} Gy^{-1}]**
pUC19, 10 ng/μl	4.2×10^5	17.983	0.3190
	1.0×10^7	3.292	0.1518
	1.0×10^8	0.589	0.0106
pBR322, 10 ng/μl	4.2×10^5	13.896	0.2752
	1.0×10^7	3.715	0.0001
	1.0×10^8	0.482	0.0003
pKLAC2, 10 ng/μl	4.2×10^5	13.776	0.4349
	1.0×10^7	3.479	0.0518
	1.0×10^8	0.555	0.0291
pUC19, 50 ng/μl	4.2×10^5	6.341	0.2026
	1.0×10^7	2.633	0.0618
	1.0×10^8	0.450	0.0006
pBR322, 50 ng/μl	4.2×10^5	4.426	0.0849
	1.0×10^7	2.018	0.0497
	1.0×10^8	0.711	0.0006
pKLAC2, 50 ng/μl	4.2×10^5	5.007	0.1757
	1.0×10^7	2.921	0.0748
	1.0×10^8	0.813	0.0027

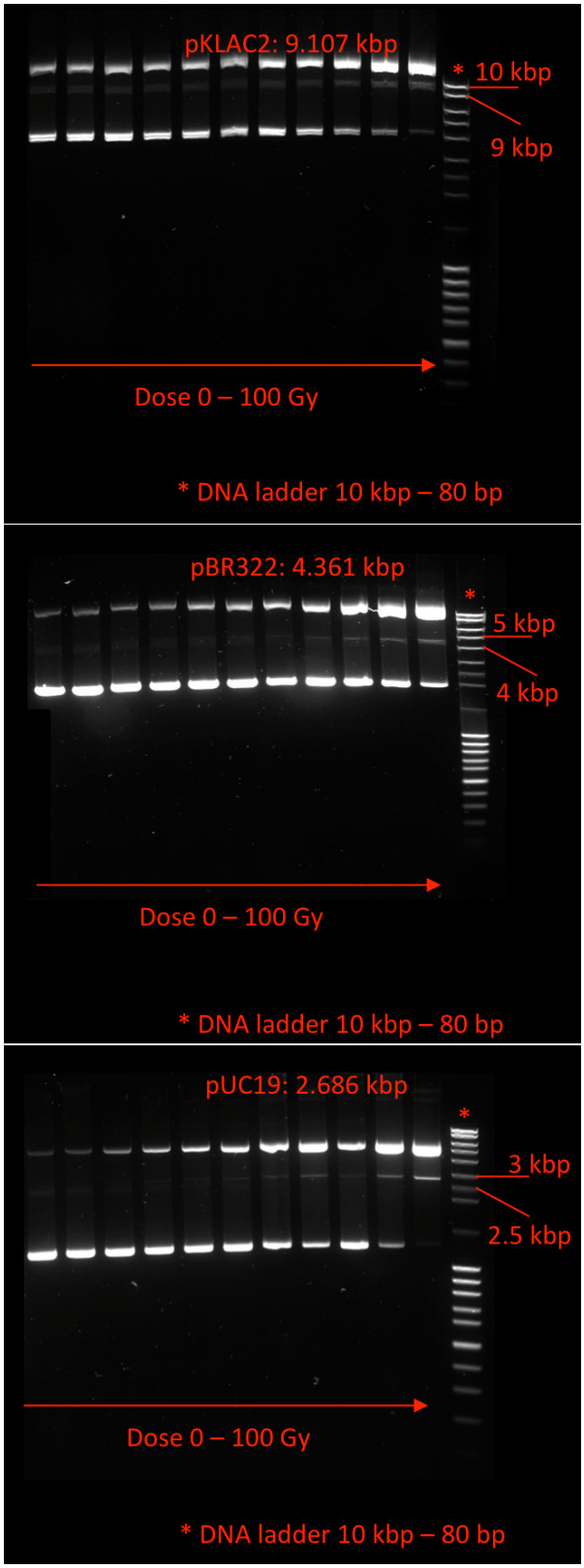

Figure 3.6: Agarose gel electrophoresis images of plasmid DNA after irradiation by 500 MeV/u Fe beam at increasing doses, starting at 0 Gy to 100 Gy. The last lane contains a DNA ladder. This example covers the samples without additive scavenger and plasmid concentrations of 10 ng/μl.

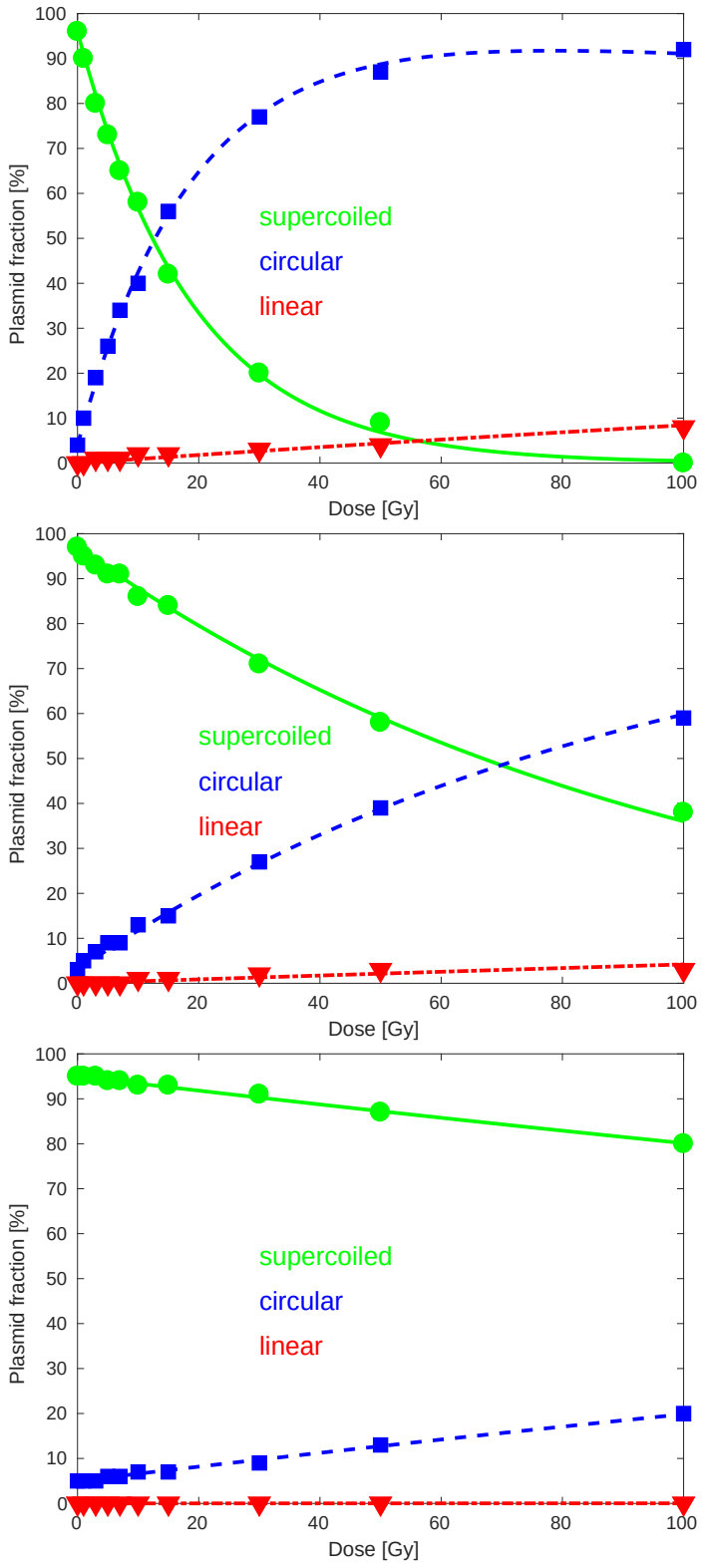

Figure 3.7: Relative yields of supercoiled, circular and linear form for pUC19 plasmid sample after 500 MeV/u Fe beam irradiation in different scavenging conditions. The scavenging capacities listed from the top to the bottom are: 4.2×10^5 s^{-1}, 1.0×10^7 s^{-1}, 1.0×10^8 s^{-1}.

Table 3.3: Radiation-induced yields of SSB and DSB per 10^6 base pairs and Gy after 400 MeV/u Ne ions irradiation for all three studied plasmids under different scavenging conditions and both used sample concentrations.

Plasmid, Concentration	**Scavenging capacity (s^{-1})**	**G (SSB) [Mbp^{-1} Gy^{-1}]**	**G (DSB) [Mbp^{-1} Gy^{-1}]**
pUC19, 10 ng/μl	4.2×10^5	24.324	0.4158
	1.0×10^7	3.534	0.1477
	1.0×10^8	1.005	0.0479
pBR322, 10 ng/μl	4.2×10^5	20.294	0.4128
	1.0×10^7	5.320	0.0303
	1.0×10^8	0.963	0.0718
pKLAC2, 10 ng/μl	4.2×10^5	16.766	0.5437
	1.0×10^7	6.198	0.0925
	1.0×10^8	1.163	0.0121
pUC19, 50 ng/μl	4.2×10^5	8.143	0.1745
	1.0×10^7	3.708	0.1198
	1.0×10^8	0.901	0.0290
pBR322, 50 ng/μl	4.2×10^5	6.512	0.1282
	1.0×10^7	3.027	0.0001
	1.0×10^8	0.642	0.0001
pKLAC2, 50 ng/μl	4.2×10^5	7.412	0.1537
	1.0×10^7	3.316	0.0662
	1.0×10^8	1.054	0.0164

Chapter 4

Discussion

4.1 Influence of various plasmid concentrations

For plasmid samples without an added scavenger we were comparing the obtained relative proportions of supercoiled, linear and circular form. We observed the following trends.

In the less concentrated solution (10 ng/μl) the relative fraction of supercoiled form decreases as a function of dose and reaches zero for all plasmid samples and all used irradiation sources at 100 Gy (the only measured non zero value being 2% in pBR322 sample irradiated with 500 MeV/u Fe ions). On the other hand, the linear form increases with dose starting at 0% in all samples except pKLAC2 where the starting point ranged from 3 – 6%. At 100 Gy it reaches 8% or 11% (when irradiated with 500 MeV/u Fe or 400 MeV/u Ne respectively) in the case of the smallest plasmid sample pUC19 and as much as 32% or 45% for our largest plasmid sample pKLAC2. With values of 10% (Fe) and 17% (Ne) for pBR322 we can assume that the linear form (linked to double strand breaks) increases with the length of a plasmid. Our numbers for ^{60}Co source irradiated samples do copy the trend of above mentioned behaviour - linear form increasing with the plasmid length up to 44% for the highest used dose.

Supercoiled plasmids have not completely vanished at 100 Gy in the more concentrated samples (50 ng/μl) after 500 MeV/u Fe irradiation - with still 14% pUC19, 13% pBR322 and 1% pKLAC2 remaining unharmed. On the contrary, no intact plasmids were detected in the same samples irradiated by ^{60}Co. 400 MeV/u Ne irradiation left 5% of pUC19, 3% of pBR322 and 0% pKLAC2 intact (4.1, 4.2. 4.3).

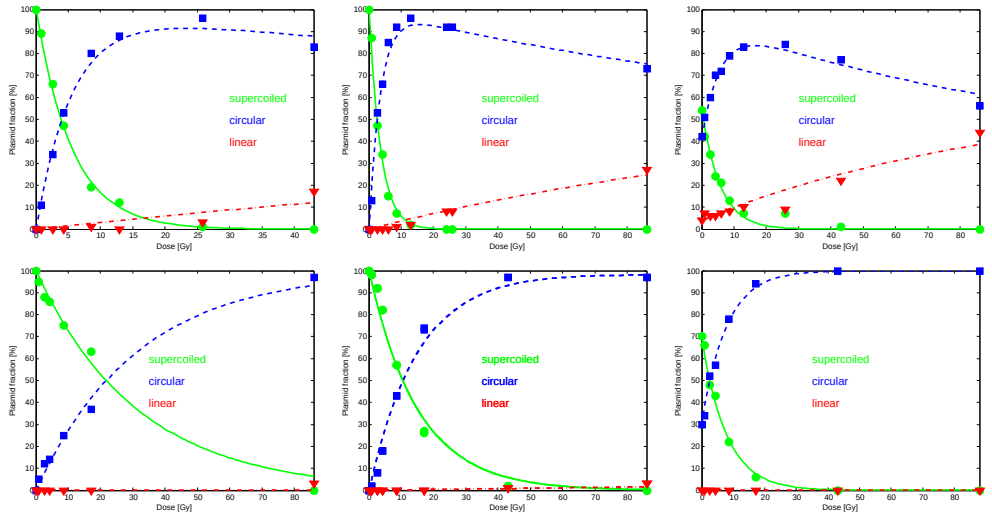

Figure 4.1: Relative yields of supercoiled, circular and linear form for plasmid samples after ^{60}Co irradiation. From left to right: pUC19, pBR322, pKLAC2. Samples diluted to concentration of 10 ng/μl are in the first row, concentration 50 ng/μl in the second.

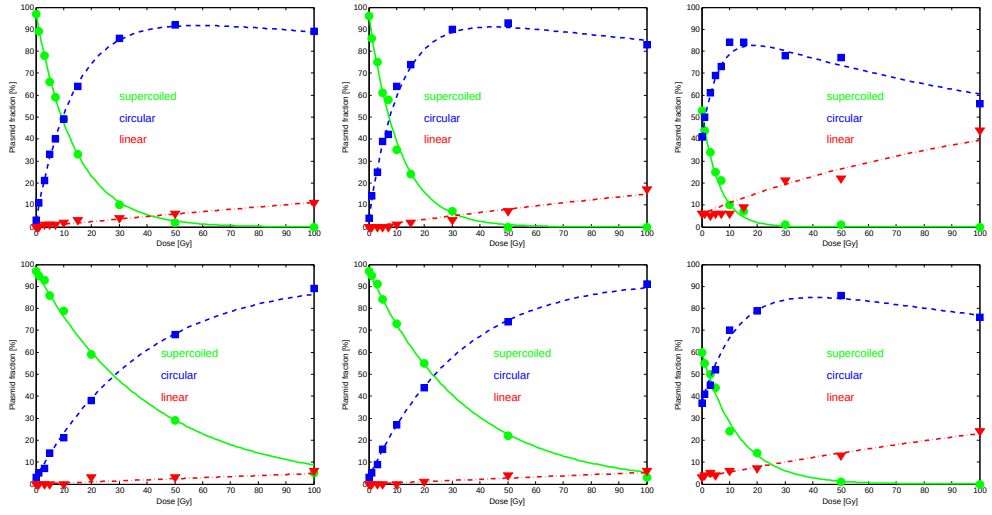

Figure 4.2: Relative yields of supercoiled, circular and linear form for plasmid samples after 400 MeV/u Ne ion beam irradiation. From left to right: pUC19, pBR322, pKLAC2. Samples diluted to concentration of 10 ng/μl are in the first row, concentration 50 ng/μl in the second.

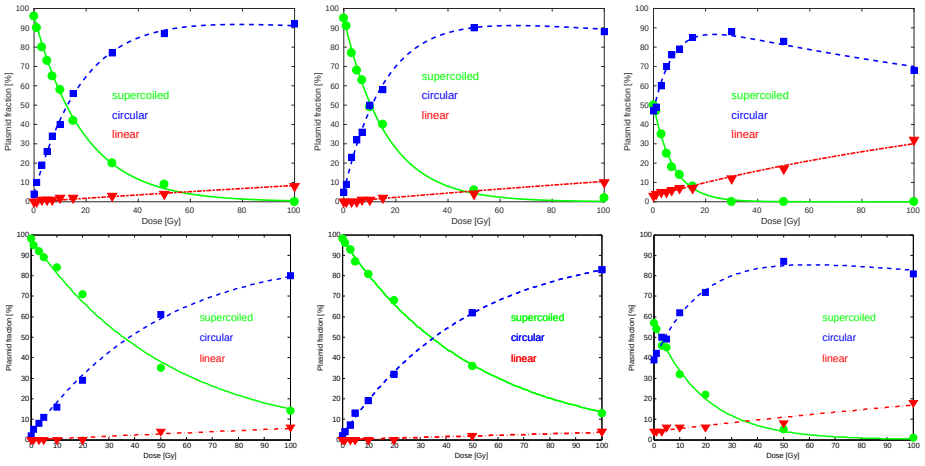

Figure 4.3: Relative yields of supercoiled, circular and linear form for plasmid samples after 500 MeV/u Fe ion beam irradiation. From left to right: pUC19, pBR322, pKLAC2. Samples diluted to concentration of 10 ng/μl are in the first row, concentration 50 ng/μl in the second.

The fraction of circular plasmids formed by single strand breaks shows an increase with dose until it reaches its maximum value. When higher doses are applied, SSBs begin to decrease at the expense of rising DSBs as the probability of a second SSB near the former one creating a DSB increases. A glimpse of this trend can for example be seen in Figure 4.4, left picture. Samples diluted to 50 ng/μl concentration would require a higher dose for the effect to be seen in our measurements.

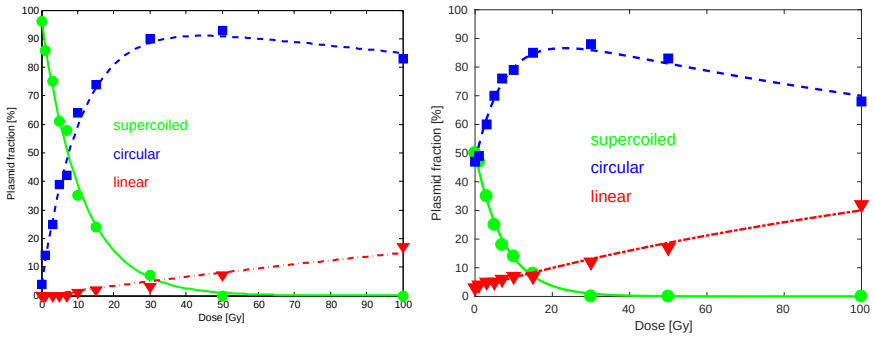

Figure 4.4: Relative yields of supercoiled, circular and linear form for pBR322 plasmid sample after 500 MeV/u Fe beam irradiation on the left and plasmid pKLAC2 sample after 500 MeV/u Fe beam on the right. Both samples diluted to a concentration of 10 ng/μl.

The data shows that pKLAC2 sample was already damaged before the irradiation, with only 50 – 54% of supercoiled form in sample concentration of 10 ng/μl and 57 – 70% of supercoiled form for 50 ng/μl.

This is the reason why we observed a distinctive decrease of the circular plasmid form at lower doses (Figure 4.4, picture on the right).

The maximum values of intact supercoiled plasmid fraction is 11% or 14% higher for the more concentrated solution for pUC19 or pBR322 irradiated with 500 MeV/u Fe ions. This difference is smaller for 400 MeV/u Ne ions with values only 0 – 5%. Such a difference is not observed for pKLAC2 plasmid sample, which can again be explained by different starting conditions as the sample was already highly damaged at the beginning. No difference at all was measured for samples irradiated with ^{60}Co.

Overall, we can conclude that both 500 MeV/u iron and 400 MeV/u neon ions are one or two orders of magnitude more effective in creating SSBs compared to DSBs for all samples and both concentrations. This is as well true for ^{60}Co irradiated and less concentrated plasmid samples. A more concentrated solution leaves the plasmids irradiated with heavy ions 2–3 times less damaged as far as SSBs are concerned. This range is wider for ^{60}Co, making it 1– 7 times. We cannot draw any such conclusions for DSBs because their calculation is more affected by the simplifications of Cowan model where fragments are neglected and the creation of DSBs by SSBs accumulation is ignored.

4.2 Influence of various scavenger concentrations

In experiments with different scavenger concentrations we can see that for all three radiation sources and all plasmid samples the linear form decreases with increasing Tris concentration to almost zero values at 100 Gy. Compared to non scavenged samples, the circular form is reduced with increasing scavenging capacity as well. The same trend is observed for both of the plasmid concentrations. This conclusion was expected - due to a longer lifetime of hydroxyl radicals at lower scavenger concentrations the probability of a radical diffusing to the target molecule and leading to a strand break is higher than in more scavenged samples. The high supercoiled fraction for high scavenger concentrations even after the plasmid was irradiated with as much as 100 Gy implies that the direct effect contribution to strand breaks is less represented compared to indirect effects through hydroxyl radicals.

When viewing the obtained data side by side one can clearly see that the addition of scavengers leads to a decrease of radiation damage. Figures 4.5, 4.6 and 4.7 show plasmid concentrations of 10 ng/μl and a similar trend is observed for plasmid concentration of 50 ng/μl.

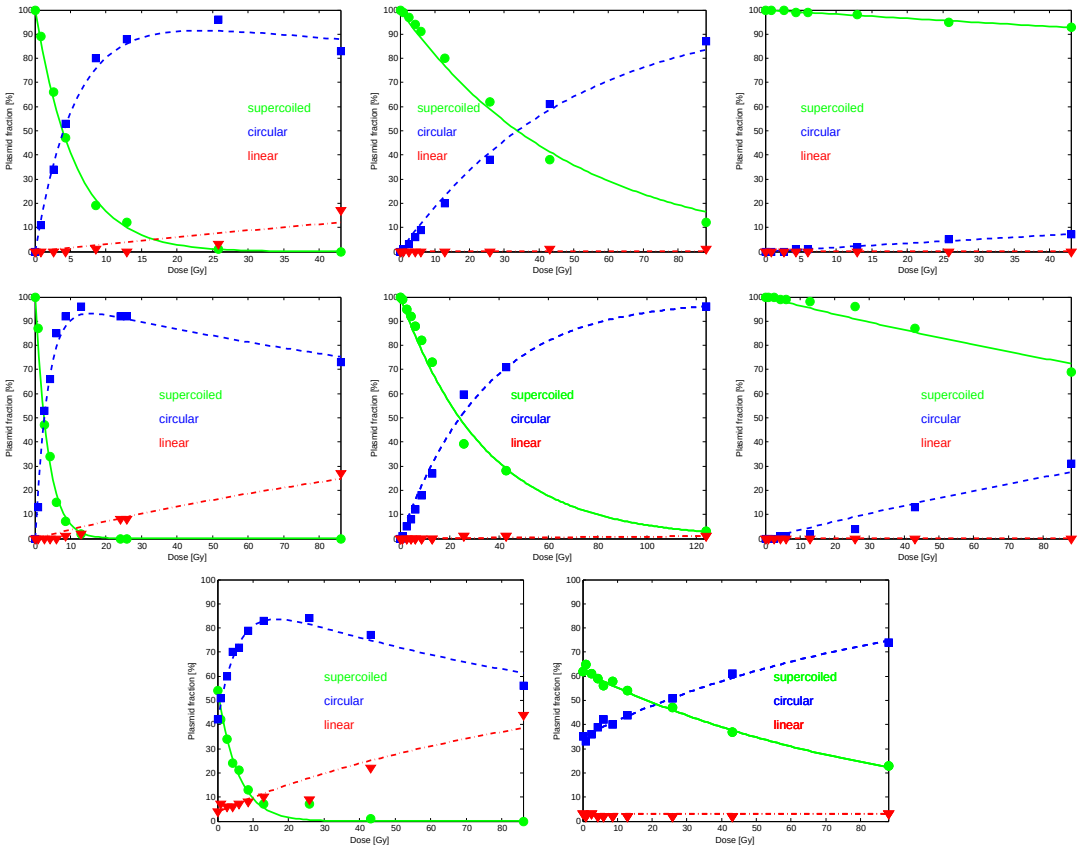

Figure 4.5: Plasmids irradiated with gamma radiation. Scavenger concentration increases from left to right: 4.2×10^5 s^{-1}, 1.0×10^7 s^{-1}, 1.0×10^8 s^{-1}. The plasmid samples listed from the top to the bottom are: pUC19, pBR322 and pKLAC2. Missing values for pKLAC2 sample with scavenger concentration of 1.0×10^7 s^{-1} are due to an error in electrophoresis apparatus settings.

Plotting G(SSB) and G(DSB) yields as a function of scavenging capacity 4.8, 4.9 and 4.10 reveals that the various DNA samples behave similarly to one another for all tested radiation sources.

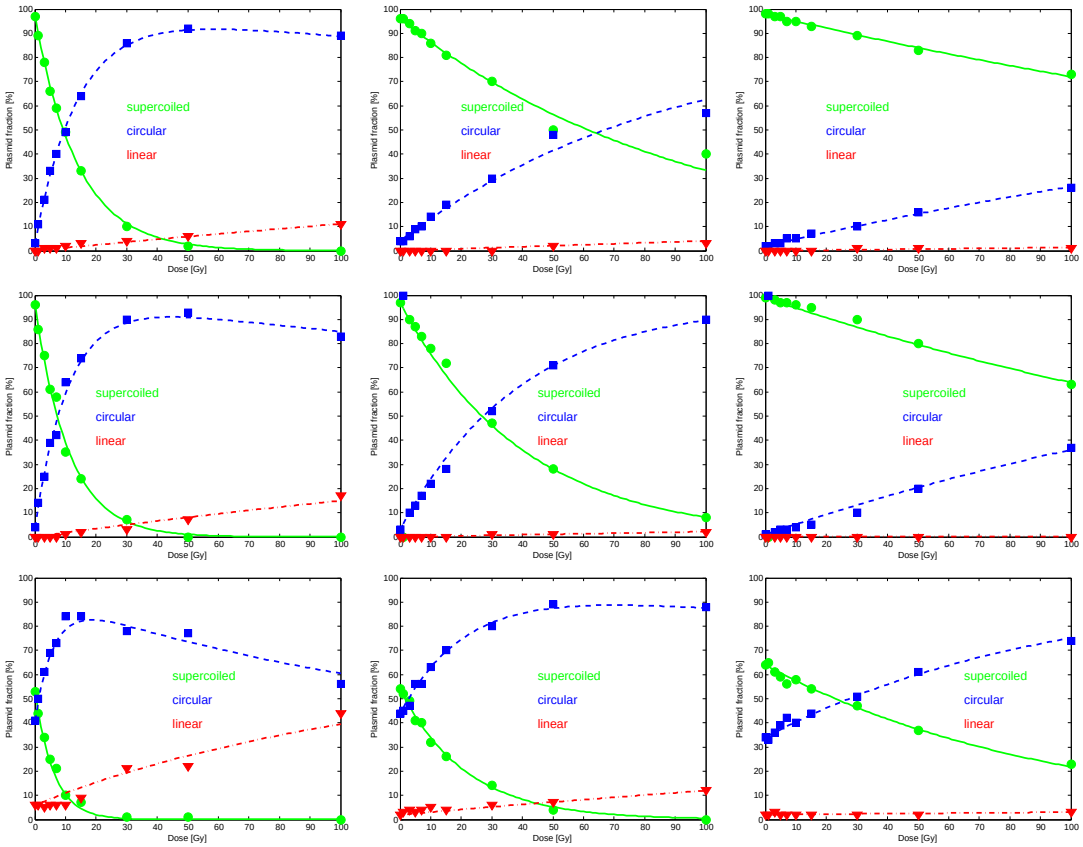

Figure 4.6: Plasmids irradiated with 400 MeV/u Ne ions. Scavenger concentration increases from left to right: 4.2×10^5 s^{-1}, 1.0×10^7 s^{-1}, 1.0×10^8 s^{-1}. The plasmid samples listed from the top to the bottom are: pUC19, pBR322 and pKLAC2.

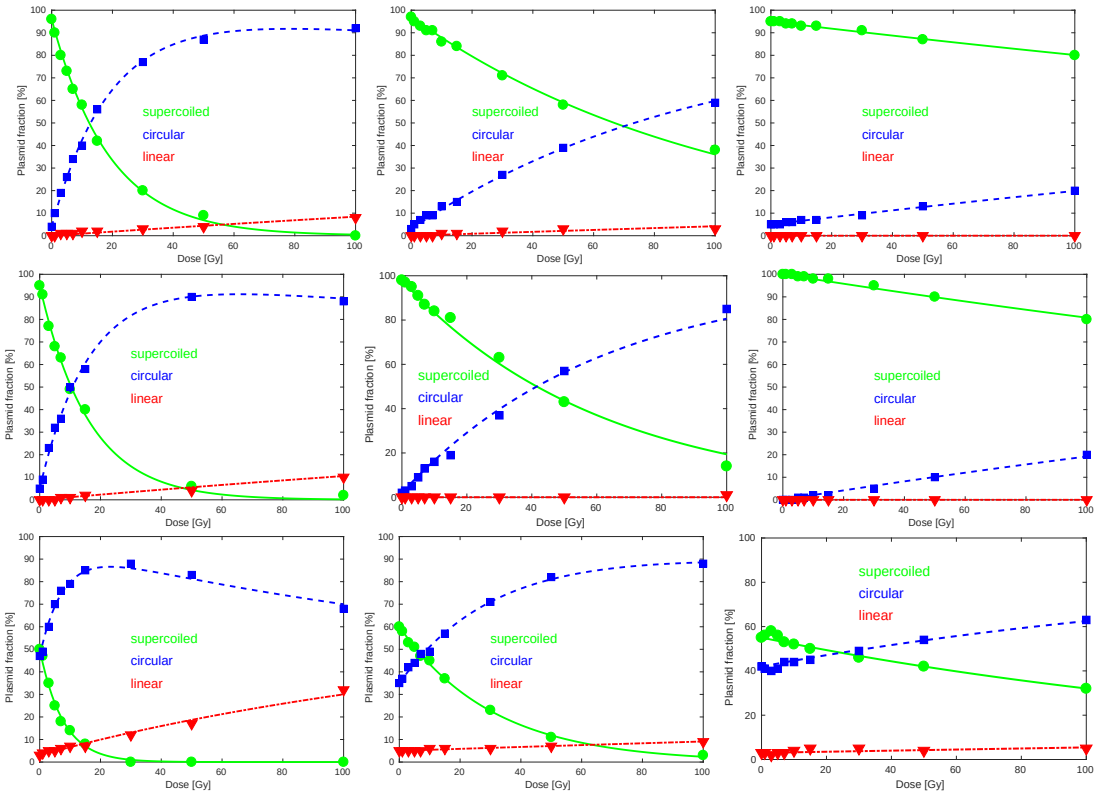

Figure 4.7: Plasmids irradiated with 500 MeV/u Fe ions. Scavenger concentration increases from left to right: 4.2×10^5 s^{-1}, 1.0×10^7 s^{-1}, 1.0×10^8 s^{-1}. The plasmid samples listed from the top to the bottom are: pUC19, pBR322 and pKLAC2.

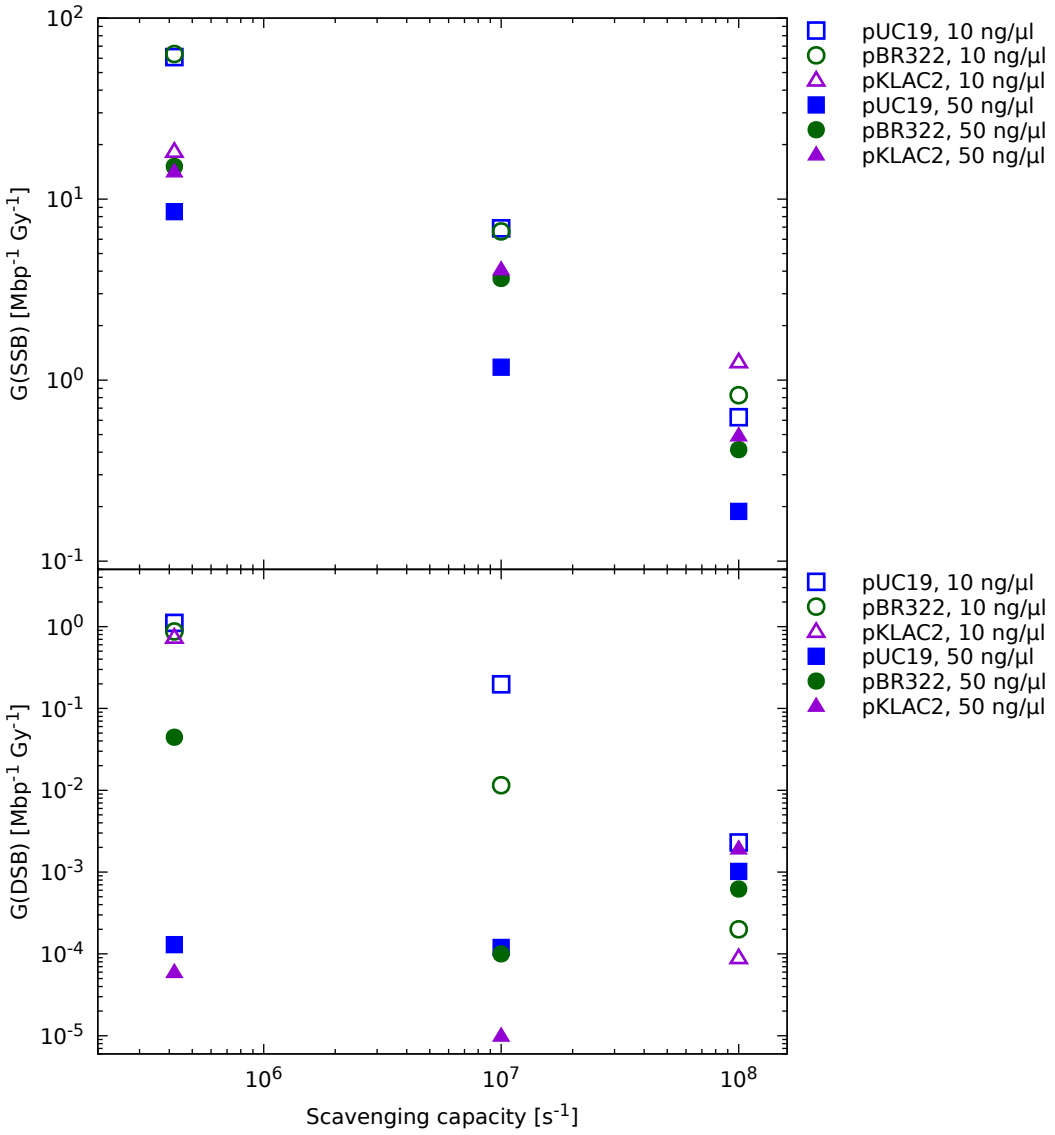

Figure 4.8: G(SSB) and G(DSB) yields induced by ^{60}Co radiation as a function of scavenging capacity. Plasmids of different lengths are marked by shape of the symbols and their concentration by full or open symbols.

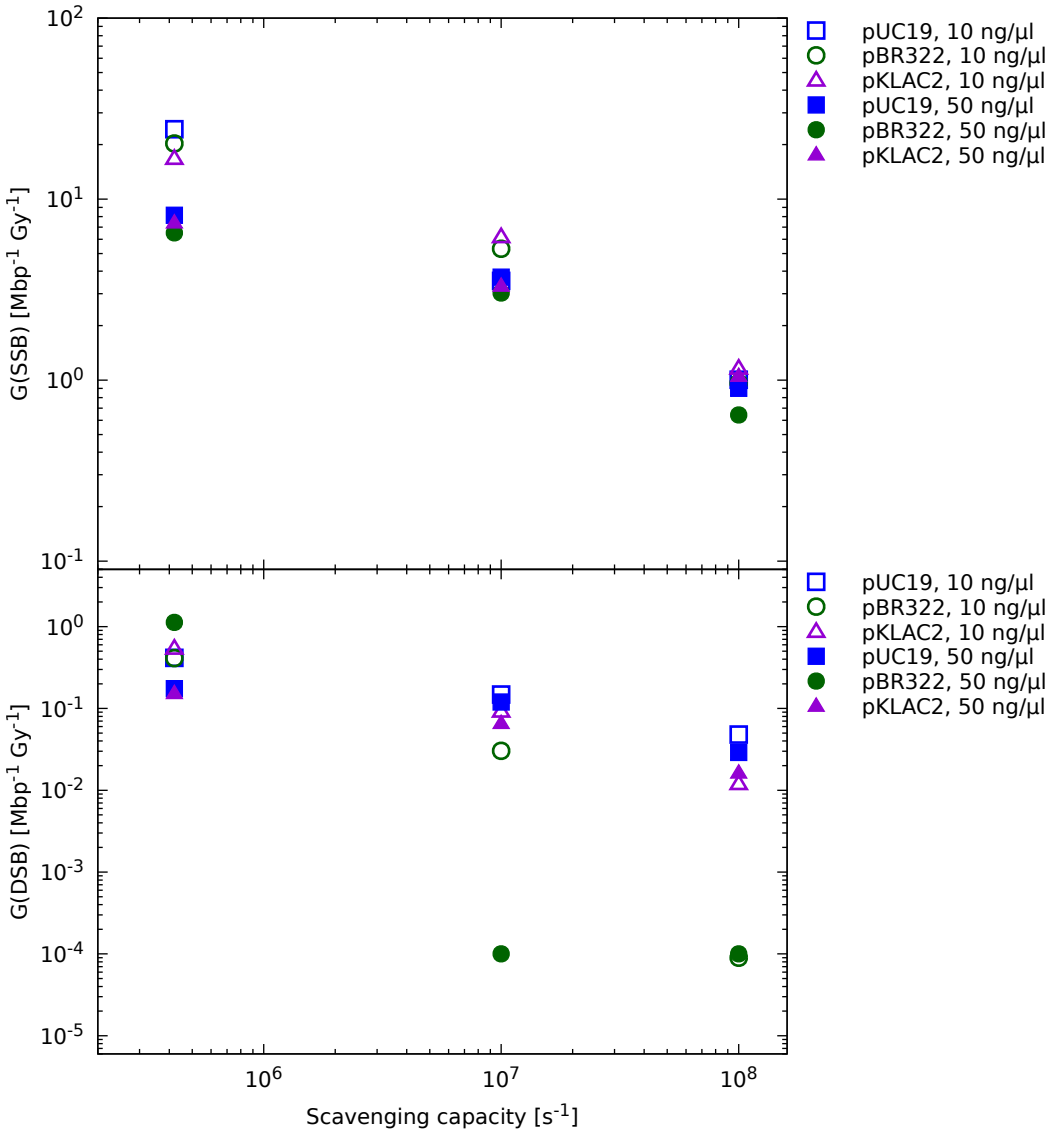

Figure 4.9: G(SSB) and G(DSB) yields induced by 400 MeV/u Ne ion radiation as a function of scavenging capacity. Plasmids of different lengths are marked by shape of the symbols and their concentration by full or open symbols.

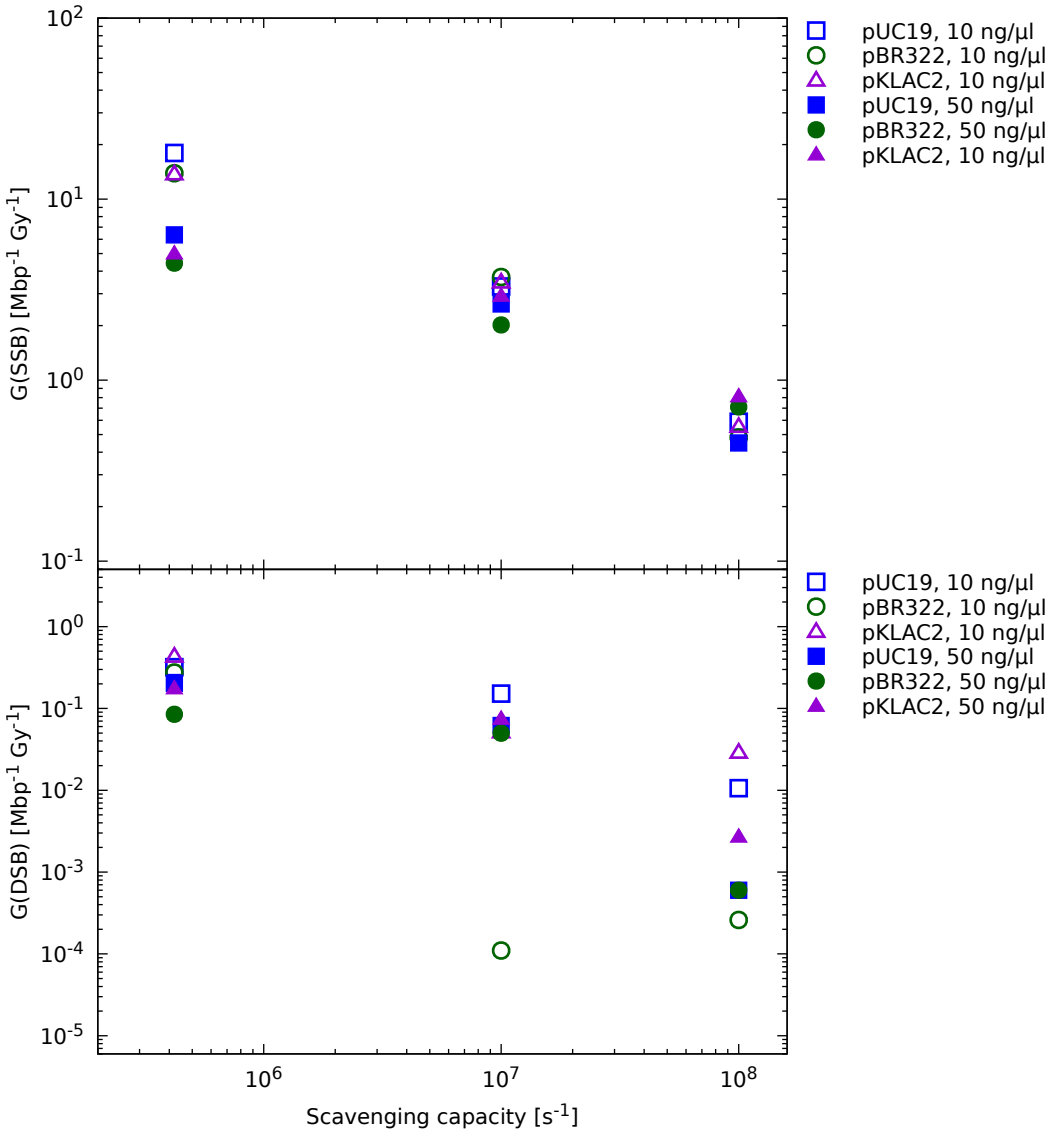

Figure 4.10: G(SSB) and G(DSB) yields induced by 500 MeV/u Fe ion radiation as a function of scavenging capacity. Plasmids of different lengths are marked by shape of the symbols and their concentration by full or open symbols.

4.2.1 Result comparison

We have compared our calculated SSB and DSB yields to a similar study of Pachnerová Brabcová, Sihver, et al. (2014) who investigated the damage to pBR322 plasmid DNA sample caused by 500 MeV/u iron beam. The plasmid was dissolved in pure water or in aqueous solution of three different scavengers (coumarin-3-carboxylic acid, dimethylsulfoxide and gylcelglycine).

The amounts of SSB we obtained were in a good agreement with the mentioned study, however DSB showed significant differences (Figure 4.11).

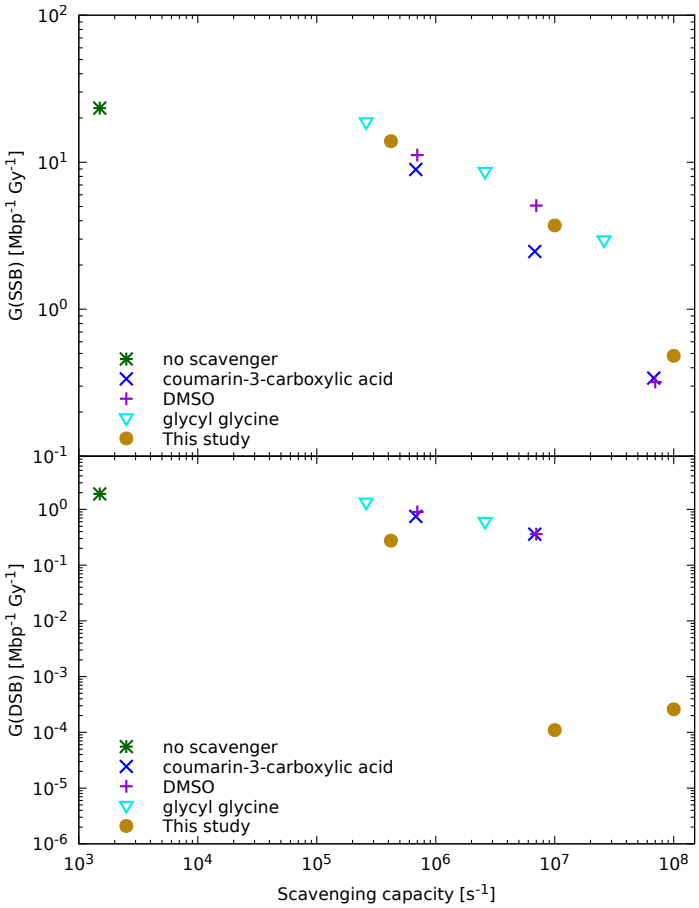

Figure 4.11: Yields of SSB and DSB induced by 500 MeV/u iron beam for different scavenging conditions.

4.3 Influence of plasmid length

As anticipated, the computed values μ and ϕ (the numbers of SSBs per molecule per Gy and DSBs per molecule per Gy respectively) confirm that the longer the plasmid, the more likely it is to be damaged. This dependence is not linear - on one hand a longer plasmid makes a better target for hydroxyl radicals, but on the other the supercoiled plasmid shape changes from "rosette-like" where few regions of the DNA double helix are in tight contact with other regions to plectonemic where the double helix interwinds for the whole length of the plasmid (Leloup et al. 2004).

This relationship observed for 500 MeV/u iron radiation source and plasmid concentration of 10 ng/μl is shown in Table 4.1. Other measured concentrations of plasmids and used radiation sources exhibit the same behaviour.

Table 4.1: computed values μ and ϕ (the numbers of SSBs per molecule per Gy and DSBs per molecule per Gy respectively.)

Plasmid, Length [bp]	**Scavenging capacity [s^{-1}]**	μ **[plasmid^{-1} Gy^{-1}]**	ϕ **[plasmid^{-1} Gy^{-1}]**
pUC19, 2886	4.2×10^5	0.0519	0.0009
	1.0×10^7	0.0095	0.0004
	1.0×10^8	0.0017	0.0000
pBR322, 4361	4.2×10^5	0.0606	0.0012
	1.0×10^7	0.0162	0.0000
	1.0×10^8	0.0021	0.0000
pKLAC2, 9107	4.2×10^5	0.1267	0.0040
	1.0×10^7	0.0320	0.0005
	1.0×10^8	0.0074	0.0000

4.4 LET dependence

It is well accepted that the LET dependence of strand break yields is linked to the number of OH radicals escaping recombination. Due to higher density of ionization for high LET radiation there is an increased intra-track recombination of those radicals which subsequently leads to less SSBs. In all radiation fields, DSBs and other clustered lesions are mainly formed by local regions of higher ionization density. At low LET these regions are widely spaced and fewer frequent than at higher LET.

As the LET increases, they become more closely spaced and may overlap, thereby increasing the size of ionization clusters and also of OH radical clusters. These clusters have the opposite influence on formation of DSBs - more ionization clusters leads to an increase of DSBs whereas their closer spacing raises the probability of radical recombination (Leloup et al. 2004).

Our data illustrate the SSB dependence on LET quite nicely. Figure 4.12 shows a decrease in the strand breaks with the increase of LET. At high scavenger concentrations the influence of the indirect effect on SSB yields weakens, which explains the milder decline of SSB yields for scavenged samples. DSBs measured in our LET range display no visible trend (Figure 4.13).

4.4.1 Result comparison

Heavy ions, which are believed to be more lethal and mutagenic than gamma rays cause less measured DNA damage in our experiment. This result seems surprising at first glance, but is in a good agreement with the theory that with increasing LET the number of SSBs is decreasing.

We have calculated how many times more SSBs and DSBs are created by gamma radiation in relation to SSBs and DSBs created by heavy ions (marked as multiplication factors f_{SSB} and f_{DSB}) and compared these ratios to corresponding data of similar studies (Table 4.2). This method allows us to make only a rough comparison because all of these studies have used either a different plasmid or ions of different LET or different scavenger type. Nevertheless, it concludes that our measurement followed the usual trend reported by others.

4.5 Uncertainty analysis

In order to get at least a rough estimate of the data variance we repeated the experiment with our three samples and gamma irradiation a second time after finishing the first set of measurements. Unfortunately, we faced a number of obstacles throughout the experiment (most notably the malfunction of UV illumination table). These have prevented us from obtaining a complete dataset. Repeated results worth reporting are in Table 4.3.

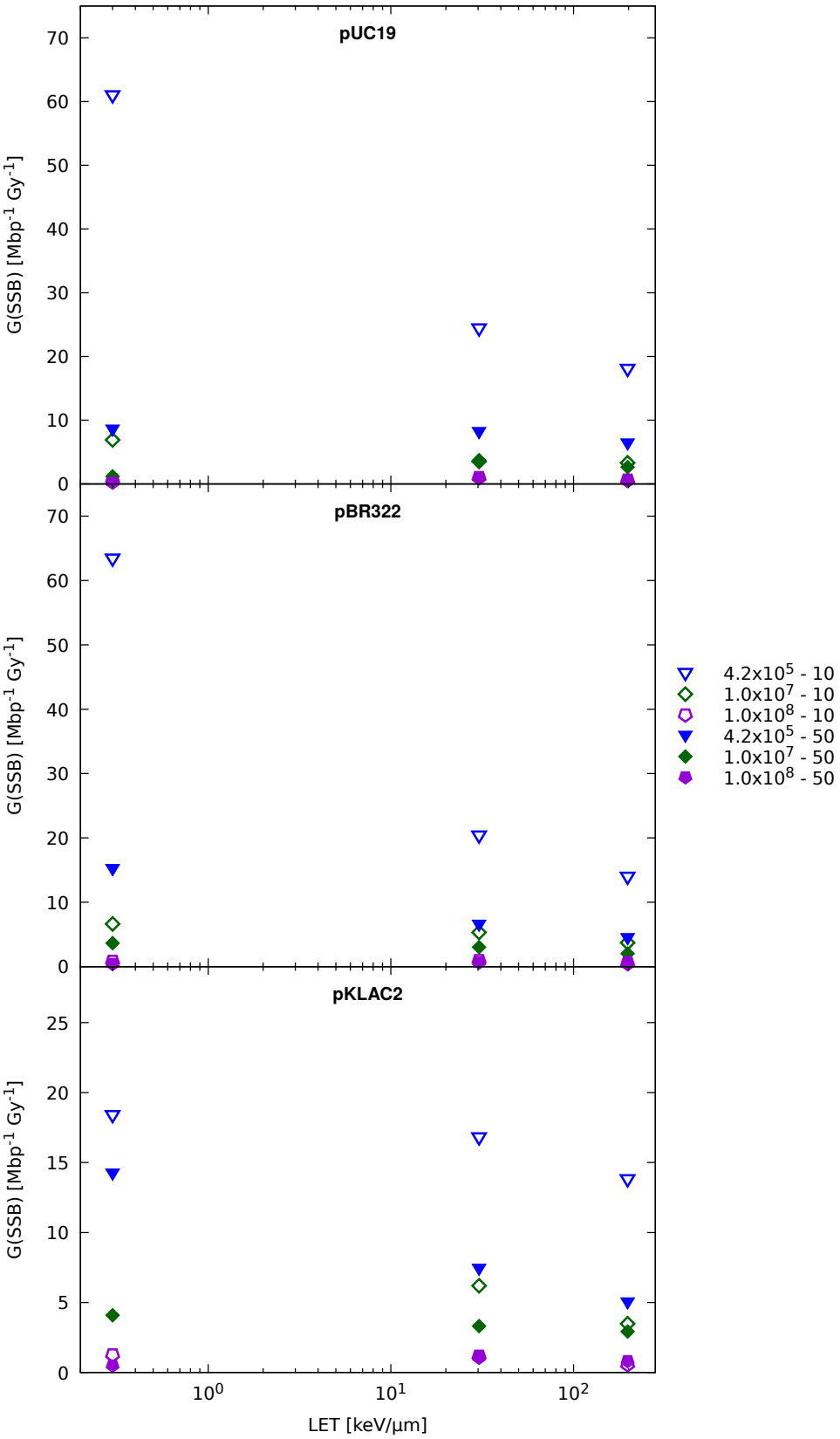

Figure 4.12: LET dependence of G(SSB) yields produced in plasmid samples of different length plotted on semi-logaritmic scale. Open symbols stand for plasmid concentration of 10 ng/μl, closed for 50 ng/μl. The shape of the symbols describes different scavenging capacities.

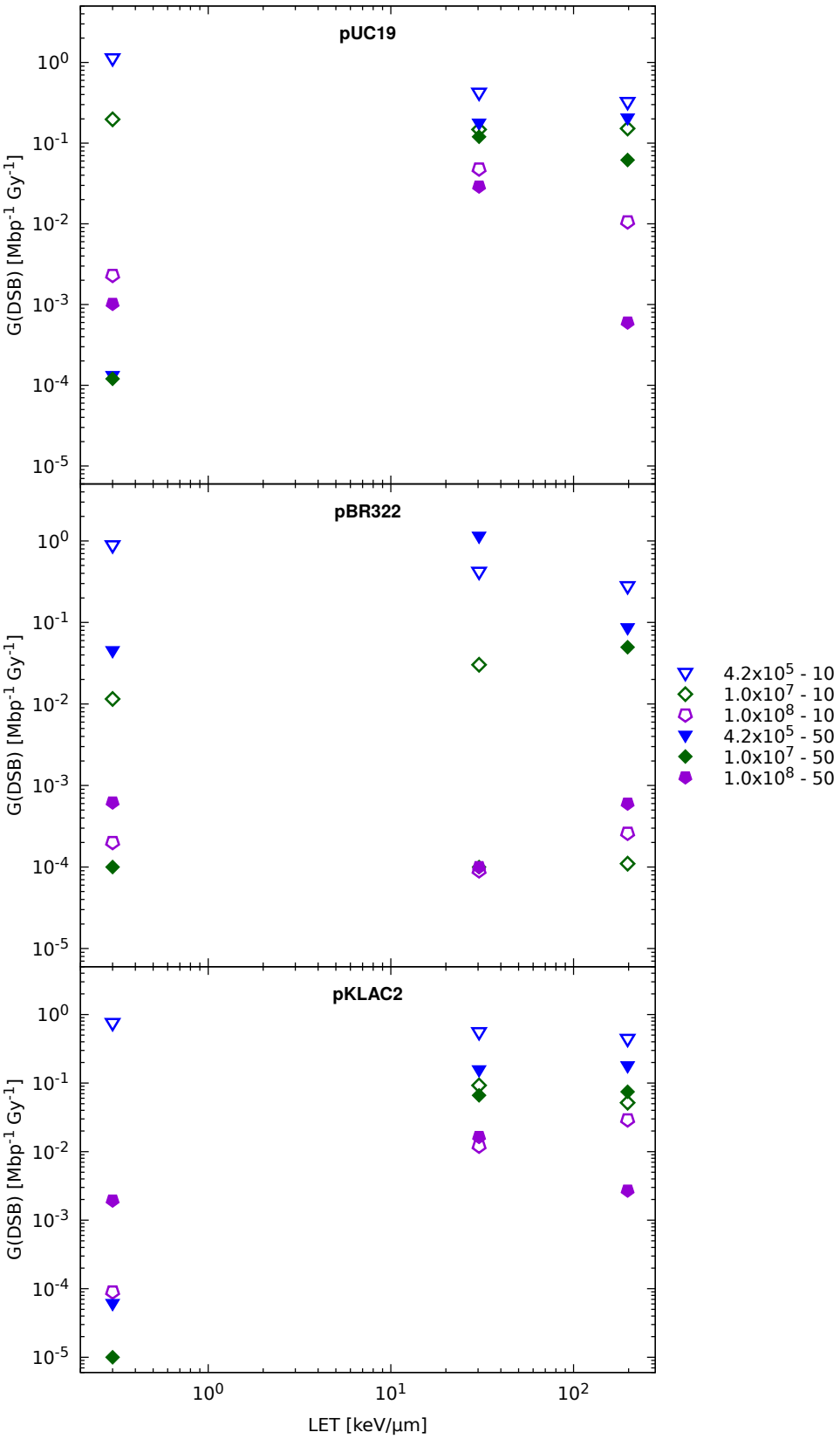

Figure 4.13: LET dependence of G(DSB) yields produced in plasmid samples of different length. Open symbols stand for plasmid concentration of 10 ng/μl, closed for 50 ng/μl. The shape of the symbols describes different scavenging capacities.

Table 4.2: Comparison of multiplication factors f_{SSB} and f_{DSB} obtained in various studies. Last column sumarizes the varying study details, "-" denotes that no added scavenger was used.

Study	$\mathbf{f_{SSB}}$	$\mathbf{f_{DSB}}$	**Study details (sample, source, scavenger)**
This study	4.6	3.2	pBR322, 500 MeV/u Fe, -
This study	3.1	2.1	pBR322, 400 MeV/u Ne, -
Taucher-Scholz et al. 1992	6.7	1.7	SV40DNA, 400 keV/μm Ne, -
Taucher-Scholz et al. 1992	2	0.7	SV40DNA, 400 keV/μm Ne,Tris
Hada and A. Georgakilas 2008	N/A	2.5	pDEL19, 200 keV/μm Fe, -
Dang et al. 2011	7.0	2.1	pBR322, 175 keV/μm ^{12}C, -
Jones et al. 1993	8	1.4	SV40DNA, 96 keV/μm ^{4}He, -
J. Milligan et al. 1996	5.6	0.7	pUC18, 102 keV/μm ^{4}He, DMSO

Table 4.3: Radiation-induced yields of SSB and DSB per 10^6 base pairs and Gy after ^{60}Co irradiation for studied plasmids under different scavenging conditions. Data obtained from a repeated measurement.

Plasmid, Concentration	**Scavenging capacity (s^{-1})**	**G (SSB) [Mbp^{-1} Gy^{-1}]**	**G (DSB) [Mbp^{-1} Gy^{-1}]**
pUC19, 10 ng/μl	4.2×10^5	73.701	0.9009
	1.0×10^7	6.687	0.0000
	1.0×10^8	0.866	0.0002
pBR322, 10 ng/μl	4.2×10^5	-	-
	1.0×10^7	8.874	0.2752
	1.0×10^8	1.949	0.2902

We have used this data from the repeated measurement to calculate uncertainty intervals which are listed listed along with our initial results in Table 4.4.

Table 4.4: Radiation-induced yields of SSB and DSB per 10^6 base pairs and Gy after ^{60}Co irradiation for studied plasmids under different scavenging conditions. Data obtained in the initial measurement with calculated uncertainty intervals.

Plasmid, Concentration	**Scavenging capacity (s^{-1})**	**G (SSB) [Mbp^{-1} Gy^{-1}]**	**G (DSB) [Mbp^{-1} Gy^{-1}]**
pUC19, 10 ng/μl	4.2×10^5	60.915 ± 9.041	1.1088 ± 0.1470
	1.0×10^7	6.896 ± 0.148	0.1975 ± 0.1397
	1.0×10^8	0.624 ± 0.171	0.0023 ± 0.0015
pBR322, 10 ng/μl	4.2×10^5	$63.334 \pm$ -	$0.8714 \pm$ -
	1.0×10^7	6.673 ± 1.556	0.0295 ± 0.1737
	1.0×10^8	0.825 ± 0.795	0.0013 ± 0.2043

The real uncertainty of our experiment will be higher, as it is a result of a number of known factors. Firstly, agarose gel electrophoresis is not able to detect short DNA fragments, which are more pronounced with increasing LET value and therefore underestimates the DNA damage. Secondly, Cowan model in its simplified form that we have used in this study has a wide range of uncertainty intervals (Pachnerová Brabcová, Jamborová, et al. 2019). Possible differences in irradiation geometry between the two experiments or damage occurred during sample storage are not significant and were neglected.

Chapter 5

Conclusions

Three different plasmid DNA were irradiated by ^{60}Co, 400 MeV/u neon ions and 500 MeV/u iron ions, either in aqueous solution or aqueous solution with different scavenger concentrations and analysed with gel electrophoresis. Samples irradiated with gamma radiation were used as an instrument for optimalization of electrophoresis gel concentrations for later use in the evaluation of plasmids irradiated with all three radiation sources.

This study has investigated the influence of two different concentrations of the plasmid samples on radiation induced SSB and DSB yields. It was confirmed that the denser concentration of a plasmid, the smaller damage was caused. Moreover, the influence of various concentrations of the hydroxyl radical scavenger Tris on the creation of SSBs and DSBs was analysed. Compared to where no scavenger is present, the DNA damage yields were reduced. This means that with a raising concentration of scavenger in the DNA solution the indirect effect of ionizing radiation through hydroxyl radicals was suppressed.

The influence of various sizes of plasmids was investigated as a part of this study as well. We had assumed that the shorter the plasmid, the smaller the probability of damage. This relation was confirmed. The dependence on LET of the ionizing radiation examined too. We obtained a dependence for SSBs that is in agreement with known theory but no trend in the DSB data was observed in the investigated LET interval.

We have compared the obtained G(SSB) and G(DSB) values of our study with a previous study by Pachnerová Brabcová, Sihver, et al. (2014). Both studies worked with pBR322 plasmid sample of equal concentration and irradiated at HIMAC facility, but with different scav-

engers and scavenging capacities. The two data sets agreed on the amounts of SSBs, but there were discrepancies in DSB yields.

There are several limitations of this study. First, the detection of DNA fragments is beyond the possibilities of agarose gel electrophoresis. A simplified Cowan model for determining SSB and DSB yields was applied where those fragments were neglected. At higher doses there is a higher probability that two and more lesions formed on the same plasmid by independent tracks will cause clustered damage. High LET radiation such as heavy ions is believed to produce high yields of clustered damage - but our simplified model takes into account only single-hit DSBs. Both effects naturally lead to an underestimation of DNA damage.

Second, DNA base damage or crosslinks leave the plasmid in supercoiled form but are still considered as radiation induced DNA damage. Unfortunately, these were not detected by our method either. This could be changed by adding base excision repair enzymes such as endonuclease III (Nth) to the plasmid samples after irradiation. The enzyme would detect a damaged base and create a strand break detectable by gel electrophoresis during the reparation process. Third, at high scavenger concentrations direct radiolysis of the scavenger may lead to formation of some highly reactive species. Another issue is that the DNA conformation may be affected by the presence of an organic solvent and this could lead to an incorrect interpretation of G(SSB) values (J. R. Milligan, Aguilera, and Ward 1993). Last but not least, the results are dependent on what model is used for estimation of μ and ϕ parameters (Vyšín et al. 2015).

To better explain the mechanism of radiation damage, mathematical modelling of DNA on atomic level and simulation of DNA damage caused by ionizing radiation has to be utilised as it goes beyond detection limits of experiments.

Bibliography

Alberts, Bruce (2002). *Molecular biology of the cell*. 4th ed. New York: Garland Science. ISBN: 0815332181.

Alpen, Edward L. (1998). *Radiation biophysics*. 2nd ed. San Diego, Calif.: Academic Press. ISBN: 978-012-0530-854.

Asaithamby, A., B. Hu, and D. J. Chen (2011). "Unrepaired clustered DNA lesions induce chromosome breakage in human cells". In: *Proceedings of the National Academy of Sciences* 108.20, pp. 8293–8298. ISSN: 0027-8424. DOI: 10.1073/pnas.1016045108.

Celeste, Arkady et al. (2003). "Histone H2AX phosphorylation is dispensable for the initial recognition of DNA breaks". In: *Nature Cell Biology* 5.7, pp. 675–679. ISSN: 1465-7392. DOI: 10.1038/ncb1004.

Chancellor, Jeffery C. et al. (2018). "Limitations in predicting the space radiation health risk for exploration astronauts". In: *Npj Microgravity* 4.1, pp. -. ISSN: 2373-8065. DOI: 10.1038/s41526-018-0043-2.

Cowan, Richard, Christina M. Collis, and Geoffrey W. Grigg (1987). "Breakage of double-stranded DNA due to single-stranded nicking". In: *Journal of Theoretical Biology* 127.2, pp. 229–245. ISSN: 00225193. DOI: 10.1016/S0022-5193(87)80133-9.

Dang, H. M. et al. (2011). "Heavy ion induced damage to plasmid DNA. plateau region vs. spread out Bragg-peak". In: *The European Physical Journal D* 63.3, pp. 359–367. ISSN: 1434-6060. DOI: 10.1140/epjd/e2011-10679-1.

Friedland, W. et al. (2017). "Comprehensive track-structure based evaluation of DNA damage by light ions from radiotherapy-relevant energies down to stopping". In: *Scientific Reports* 7.1. ISSN: 2045-2322. DOI: 10.1038/srep45161.

Georgakilas, Alexandros G., Peter O'Neill, and Robert D. Stewart (2013). "Induction and Repair of Clustered DNA Lesions. What Do We Know So Far?" In: *Radiation Research* 180.1, pp. 100–109. ISSN: 0033-7587. DOI: 10.1667/RR3041.1.

Glasel, Jay A. and Murray P. Deutscher (1995). *Introduction to biophysical methods for protein and nucleic acid research*. 1st. San Diego: Academic Press. ISBN: 0122862309.

Hada, Megumi and Alexandros G. Georgakilas (2008). "Formation of Clustered DNA Damage after High-LET Irradiation. A Review". In: *Journal of Radiation Research* 49.3, pp. 203–210. ISSN: 0449-3060. DOI: 10.1269/jrr.07123.

Hall, Eric J. and Amato J. Giaccia (2006). *Radiobiology for the radiologist*. 6th ed. Philadelphia: Lippincott Williams & Wilkins. ISBN: 0781741513.

Higgins, N. Patrick and Alexander V. Vologodskii (2015). "Topological Behavior of Plasmid DNA". In: *Microbiology Spectrum* 3.2. ISSN: 2165-0497. DOI: 10.1128/microbiolspec.PLAS-0036-2014.

Hodgkins, Paul S., Micaela P. Fairman, and Peter O'Neill (1996). "Rejoining of Gamma-Radiation-Induced Single-Strand Breaks in Plasmid DNA by Human Cell Extracts. Dependence on the Concentration of the Hydroxyl Radical Scavenger, Tris". In: *Radiation Research* 145.1, pp. 24–30. ISSN: 00337587. DOI: 10.2307/3579191.

Hutchinson, Franklin (1985). "Chemical Changes Induced in DNA by Ionizing Radiation". In: *Progress in Nucleic Acid Research and Molecular Biology Volume 32*. Elsevier, pp. 115–154. ISBN: 9780125400329. DOI: 10.1016/S0079-6603(08)60347-5.

Jones, G. D. D. et al. (1993). "Yield of Strand Breaks as a Function of Scavenger Concentration and LET for SV40 Irradiated with 4 He Ions". In: *Radiation Research* 136.2. ISSN: 00337587. DOI: 10.2307/3578610.

Kavanagh, Joy N. et al. (2013). "DNA Double Strand Break Repair. A Radiation Perspective". In: *Antioxidants & Redox Signaling* 18.18, pp. 2458–2472. ISSN: 1523-0864. DOI: 10.1089/ars.2012.5151.

Klimczak, U. et al. (2009). "Irradiation of Plasmid and Phage DNA in Water—alcohol Mixtures. Strand Breaks and Lethal Damage as a Function of Scavenger Concentration". In: *International Journal of Radiation Biology* 64.5, pp. 497–510. ISSN: 0955-3002. DOI: 10.1080/09553009314551711.

Lee, Pei Yun et al. (2012). "Agarose Gel Electrophoresis for the Separation of DNA Fragments". In: *Journal of Visualized Experiments* 62, pp. -. ISSN: 1940-087X. DOI: 10.3791/3923.

Lehnert, Shirley (2008). *Biomolecular action of ionizing radiation*. New York: Taylor & Francis. ISBN: 978-0750308243.

Leloup, C et al. (2004). "Evaluation of lesion clustering in irradiated plasmid DNA". In: *International Journal of Radiation Biology* 81.1, pp. 41–54. ISSN: 0955-3002. DOI: 10.1080/09553000400017895.

Medicine, Institute of and National Research Council (2014). *Research on Health Effects of Low-Level Ionizing Radiation Exposure: Opportunities for the Armed Forces Radiobiology Research Institute*. Washington, DC: The National Academies Press. ISBN: 978-0-309-30209-8. DOI: 10.17226/18732.

Milligan, J. R., J. A. Aguilera, and J. F. Ward (1993). "Variation of Single-Strand Break Yield with Scavenger Concentration for Plasmid DNA Irradiated in Aqueous Solution". In: *Radiation Research* 133.2, pp. 151–. ISSN: 00337587. DOI: 10.2307/3578350.

Milligan, J. R. et al. (1996). "The Difference That Linear Energy Transfer Makes to Precursors of DNA Strand Breaks". In: *Radiation Research* 145.4. ISSN: 00337587. DOI: 10.2307/3579065.

Pachnerová Brabcová, Kateřina, Zuzana Jamborová, et al. (2019). "Radiation-induced plasmid DNA damage: effect of concentration and length". In: *Accepted to: Radiation Protection Dosimetry* -.

Pachnerová Brabcová, Kateřina, Lembit Sihver, et al. (2014). "Clustered DNA damage on subcellular level. effect of scavengers". In: *Radiation and Environmental*

Biophysics 53.4, pp. 705–712. ISSN: 0301-634X. DOI: 10.1007/s00411-014-0557-2.

Pachnerová Brabcová, Kateřina, Václav Štěpán, et al. (2017). "Fading of CaSO 4 thermoluminescent detectors after exposure to charged particles". In: *Radiation Measurements* 106.106, pp. 569–572. ISSN: 13504487. DOI: 10.1016/j.radmeas.2017.02.002.

Pray, L. (2008). *Discovery of DNA Structure and Function: Watson and Crick. Nature Education*. URL: https://www.nature.com/scitable/topicpage/discovery-of-dna-structure-and-function-watson-397 (visited on 08/28/2018).

PRCOG (2019). *Particle Therapy Co-Operative group*. URL: https://ptcog.ch/index.php/facilities-in-operation (visited on 2019).

Takatsuji, Toshihiro, Isao Yoshikawa, and Masao S. Saski (1999). "Generalized Concept of the LET-RBE Relationship of Radiation-induced Chromosome Aberration and Cell Death". In: *Journal of Radiation Research* 40.1, pp. 59–69. ISSN: 04493060. DOI: 10.1269/jrr.40.59.

Taucher-Scholz, G. et al. (1992). "Induction of DNA breaks in SV40 by heavy ions". In: *Advances in Space Research* 12.2-3, pp. 73–80. ISSN: 02731177. DOI: 10.1016/0273-1177(92)90093-D.

Terato, H. et al. (2014). "Quantitative characteristics of clustered DNA damage in irradiated cells by heavy ion beams". In: *Journal of Radiation Research* 55.suppl 1, pp. i89–i90. ISSN: 0449-3060. DOI: 10.1093/jrr/rrt173.

von Sonntag, C. (2006). *Free-radical-induced DNA damage and its repair. a chemical perspective*. 1st. Berlin: Springer. ISBN: 3-540-26120-6.

Vyšín, Luděk et al. (2015). "Proton-induced direct and indirect damage of plasmid DNA". In: *Radiation and Environmental Biophysics* 54.3, pp. 343–352. ISSN: 0301-634X. DOI: 10.1007/s00411-015-0605-6.

Watson, J. D. and F. H. C. Crick (1953). "Molecular Structure of Nucleic Acids. A Structure for Deoxyribose Nucleic Acid". In: *Nature* 171.4356, pp. 737–738. ISSN: 0028-0836. DOI: 10.1038/171737a0.

Zhu, Xiaoying et al. (2010). "Effect of crowding on the conformation of interwound DNA strands from neutron scattering measurements and Monte Carlo simulations". In: *Physical Review E* 81.6, E 81. ISSN: 1539-3755. DOI: 10.1103/PhysRevE.81.061905.